

Manuscript Title: Plasma membrane phosphatidylinositol 4-phosphate and 4,5-bisphosphate determine the distribution and function of K-Ras4B but not H-Ras proteins

Manuscript No: JBC/2017/806679 [R1]

Manuscript Type: Regular Paper

Date Submitted by the Author: 11 Sep 2017

Complete List of Authors: Gergo Gulyas, Gloria Radvanszki, Rita Matuska, Andras Balla, Laszlo Hunyady, Tamas Balla, and Peter Varnai

Keywords: bioluminescence resonance energy transfer (BRET); G protein-coupled receptor (GPCR) ; Golgi; GTPase Kras (KRAS); phosphoinositide

Plasma membrane phosphatidylinositol 4-phosphate and 4,5-bisphosphate determine the distribution and function of K-Ras4B but not H-Ras proteins

Gergő Gulyás¹, Glória Radvánszki¹, Rita Matuska¹, András Balla^{1,2}, László Hunyady^{1,2}, Tamas Balla³ and Péter Várnai^{1#}

¹Department of Physiology, Faculty of Medicine, Semmelweis University, Budapest, Hungary

²MTA-SE Laboratory of Molecular Physiology, Budapest, Hungary

³Section on Molecular Signal Transduction, Eunice Kennedy Shriver National Institute of Child Health and Human Development, National Institutes of Health, Bethesda, MD, USA

Running title: K-Ras trafficking

#Corresponding author: Péter Várnai, MD, PhD, DSc, Department of Physiology, Faculty of Medicine, Semmelweis University, Budapest, P. O. Box 259, H-1444 Budapest, Hungary
e-mail: varnai.peter@med.semmelweis-univ.hu

Keywords: K-Ras, Phosphoinositides, Golgi, GPCR, BRET

Abstract

Plasma membrane (PM) localization of Ras proteins is crucial for transmitting signals upon mitogen stimulation. Posttranslational lipid modification of Ras proteins plays an important role in their recruitment to the PM. Electrostatic interactions between negatively charged PM phospholipids and basic amino acids found in K-Ras4B (K-Ras) but not in H-Ras are important for permanent K-Ras localization to the PM. Here, we investigated how acute depletion of negatively charged PM polyphosphoinositides (PPIs) from the PM alters the intracellular distribution and activity of K- and H-Ras proteins. PPIs depletion from the PM was achieved either by agonist-induced activation of phospholipase C β (PLC β) or with a rapamycin-inducible system in which various PI phosphatases were recruited to the PM. Redistribution of the two Ras proteins was monitored with confocal microscopy or with a recently developed bioluminescent energy transfer (BRET)-based approach involving fusion of the Ras C-terminal targeting sequences or the entire Ras proteins to Venus fluorescent protein. We found that PM PPIs depletion caused rapid translocation of K-Ras but not H-Ras from the PM to the Golgi. PM depletion of either

phosphatidylinositol 4-phosphate (PtdIns4P) or PtdIns(4,5)P₂, but not PtdIns(3,4,5)P₃, was sufficient to evoke K-Ras translocation. This effect was diminished by deltarasine, an inhibitor of the Ras–phosphodiesterase interaction, or by simultaneous depletion of the Golgi PtdIns4P. The PPIs depletion decreased incorporation of [³H]-Leucine in K-Ras-expressing cells, suggesting that Golgi-localized K-Ras is not as signaling competent as its PM-bound form. We conclude that PPIs in the PM are important regulators of K-Ras mediated signals.

The interaction of intracellular signaling proteins with the hydrophobic membranes of eukaryotic cells is critical for the signaling competence of these proteins. In the case of the peripheral PM proteins, such interaction with the PM can occur via different mechanisms. Proteins that contain an amphipathic α -helix or hydrophobic loops can directly penetrate into the inner surface of the membrane. Others, however, do not contain enough clustered hydrophobic amino acids to maintain a stable membrane interaction. In this case other mechanisms are necessary to attach the protein to the PM. Many signaling proteins undergo post-translational lipid modifications, attaching a

myristoyl, palmitoyl or prenyl group on specific amino acid residues. These modifications provide the lipophilicity of the proteins ensuring proper PM localization (1).

Ras protein mutations are one of the most common causes in cancer and hence have attracted a lot of attention. These small globular proteins are molecular switches that change conformation upon GTP binding relative to their GDP-bound forms (2,3). Their C-termini contain their localization signal providing for membrane attachment due to post-translational modifications. Numerous oncogenic mutations of Ras proteins have been identified, many of which affect GTP binding of these proteins, but naturally occurring mutations in the C-terminal anchoring domains have not been reported yet, showing the uniquely significant role of this conserved essential segment of the Ras protein functions (4). H-Ras proteins undergo two lipid modifications: in addition to their C-terminal prenylation, they are also palmitoylated in their C-terminal tails (5). In contrast, K-Ras protein contain only the prenyl modification and their PM anchoring is highly dependent on a polybasic amino acid sequence as a „second signal” located in their C-terminal tail (6). Previous studies have shown that changing the positively charged amino acids to neutral amino acids by site directed mutagenesis can fully abolish the PM localization of the K-Ras protein. Such mutated K-Ras proteins show non-specific endomembrane localization similarly to that of proteins that have only a prenyl or myristoyl group as targeting signals (7-9).

At cytoplasmic pH, the cytosolic face of the PM is enriched in two types of anionic phospholipids: phosphatidylserine (PS) is the most abundant anionic phospholipid, amounting to 3-10% of the total phospholipid pool of the cells (10) found in the inner leaflet of the PM. The other is the various polyphosphoinositides (PPIs) that account less than 1% of total anionic phospholipids (11). Although PS is found in a relative high amount in the PM providing the bulk negativity for the inner leaflet of the membrane (12), its precise role in controlling cellular processes is vastly under-explored. In contrast, the impact of the PPIs in the regulation of variety of cellular processes is well established. Of the three PPIs phosphatidylinositol 4-phosphate (PtdIns4P) and phosphatidylinositol 4,5-bisphosphate (PtdIns(4,5)P₂) equally share the majority role, whereas phosphatidylinositol 3,4,5-

trisphosphate (PtdIns(3,4,5)P₃) is present only in a very small amount even in stimulated cells. While these lipids have substantial roles in the regulation of ion channels, cell motility, vesicular trafficking, and they also represent molecular clues for targeting signaling proteins to membranes (13-15), their contribution to the regulation of some important pathways is not fully explored.

In this study, we investigated how the rapid depletion of PM PPIs can regulate the intracellular distribution of lipid anchored PM proteins, namely the K- and H-Ras proteins. Using a BRET-based method suitable to monitor the movement of PM bound proteins after they are released from the PM, we show the translocation of K-Ras or its isolated targeting sequence to either the ER or the Golgi upon rapid PM PPIs depletion. The method is highly sensitive, can be easily quantified, therefore, allows the comparison of the involvement of the various PPIs in the PM localization of the Ras proteins. This analysis also reveals that PM PPIs depletion significantly attenuates the proliferation of the cells expressing constitutively active K- but not H-Ras mutants, which highlights the different functional role of the PPIs dependent PM anchoring in K-Ras and H-Ras signaling.

Results

Energy transfer-based monitoring of the intracellular movement of peripheral proteins bound to the cytoplasmic surface of the PM

We designed several constructs to target the Venus protein to the inner leaflet of the PM using targeting signal sequences either added to the N- or the C-termini of the fluorescent protein (Fig. 1A). These included the N-terminal 14 amino acids of the Lyn kinase, which has a single palmitoyl and a single myristoyl modification (Lyn₁₋₁₄-Venus), the N-terminal 10 amino acids of the Lck kinase, which has a double palmitoyl and a single myristoyl residue (Lck₁₋₁₀-Venus), and the N-terminal 15 amino acids of the c-Src kinase, which contains only a single myristoyl (c-Src₁₋₁₅-Venus). As for C-terminal signal sequences, we used the C-terminal 22 residues of K-Ras modified by prenylation (Venus-K-Ras-CAAX), or the C-terminal 22 amino acid signal sequence of the H-Ras, which possesses double palmitoylation and prenylation (Venus-H-Ras-CAAX). Notably, in addition to the lipid

modification, the targeting sequences of c-Src and K-Ras also contained a number of positively charged amino acids. As expected and showed before by various reports (14,16,17), transient expression of all of these constructs in HEK 293T cells labeled the PM (Fig. 1A). Importantly, most of the constructs also displayed a small but consistent endomembrane localization, the amount of which was minimal relative to the total amount of the proteins.

Recently we developed a bioluminescent energy transfer (BRET)-based method monitoring the proximity of luciferase-tagged PM receptors and the Venus protein targeted to the surface of various intracellular organelles. This method was successfully used to follow the intracellular trafficking route of GPCRs from the PM to different intracellular compartments (18,19). To investigate the dynamic changes of the membrane localization of peripheral membrane proteins that bind the PM, and follow their intracellular fates, we utilized the same approach with some modifications. The most important modification was that now we targeted the luciferase enzyme itself to the cytoplasmic surface of the different intracellular organelles to serve as donor and used the Venus protein tagged with the various PM-targeting sequences (see above) as the acceptor (Fig. 1B).

Moreover, we used an improved version of Renilla luciferase and fused it to well characterized resident protein sequences defining various organelles. These included targeting sequences of TGN38 (N-terminal target of the full length protein) for Golgi, TOM70 (N-terminal 1-30 amino acids) for mitochondria, Sac1 (C-terminal 521-587 amino acids) for ER and EEA1 (1253-1411 amino acids that corresponds its FYVE-domain) for early endosomes (Fig. 1C). To validate proper localization, Luciferase enzyme was replaced by Cerulean in all of the constructs, and the constructs were expressed in HEK 293T cells to confirm their proper localization (Fig. 1C).

Acute manipulation of PM PPIs pools

To achieve the PM PPIs depletion, a previously described rapamycin-induced heterodimerization system was used (20). In most of the experiments, the FKBP-fused version of the bifunctional phosphatase, Pseudojanin (PJ) containing a 4- and a 5-phosphatase domain (15). FRB was targeted to the PM using the targeting sequence of the Lck

protein (Fig. 2A). When the role of PtdIns(3,4,5) P_3 was studied, low (100 nM) concentration of wortmannin was used to inhibit Class I PtdIns 3-kinase activity.

Effects of these manipulations on PM PPIs levels were validated using specific biosensors based on the following lipid binding domains: SidM-2xP4M as the PtdIns4P sensor (21), PLC δ_1 -PH as the PtdIns(4,5) P_2 sensor (22) and Btk-PH as the PtdIns(3,4,5) P_3 sensor (23). As shown on Fig. 2B by confocal microscopy in HEK 293T cells rapamycin-induced PJ recruitment resulted in the decrease in both the PtdIns4P and PtdIns(4,5) P_2 levels. This was confirmed by using the more quantitative BRET-based biosensors (24). Recruitment of PJ enzymes of various activities with 300 nM rapamycin resulted in a rapid decrease of the PM PtdIns4P, PtdIns(4,5) P_2 and PtdIns(3,4,5) P_3 (Fig. 2C red curves). Wortmannin pretreatment did not affect the PM PtdIns4P, PtdIns(4,5) P_2 , but induced maximal depletion of PM PtdIns(3,4,5) P_3 . Notably, wortmannin treatment reduced PM PtdIns(3,4,5) P_3 to a lower level than the rapamycin-induced depletion of its precursor, PtdIns(4,5) P_2 , indicating that the removal of the PtdIns(3,4,5) P_3 precursor may not have been complete and the inhibition of the PI3Ks enzyme is more effective under these conditions. Although these results were mostly confirmatory of previous similar studies, they were important for proper evaluation of the subsequent experiments.

PM PPIs depletion evokes the redistribution of the polybasic peripheral proteins from the PM to the Golgi

Hammond et al. have found that peripheral proteins containing positively charged amino acids are released from the PM after combined PtdIns4P and PtdIns(4,5) P_2 depletion (15). To investigate this phenomenon in further details using the various PM-targeted Venus, we initially performed confocal measurements. As shown on Fig. 3A, depletion of PM PtdIns4P, PtdIns(4,5) P_2 and PtdIns(3,4,5) P_3 level by the addition of rapamycin clearly reduced the PM localization of Venus-K-Ras-CAAX, while the localization of the other PM targeted Venus constructs (Lyn $_{1-14}$ -Venus, Lck $_{1-10}$ -Venus, Venus-H-Ras-CAAX) remained unchanged (Fig. 3A). In the case of the c-Src $_{1-15}$ -Venus the reduction of PM localization is not so clear, but there is a tendency that the fluorescent signal

showed an endomembrane pattern upon rapamycin treatment (Fig. 3A).

To obtain more information about the fate of the proteins after their release from the PM, we next performed BRET measurement between the proteins and various intracellular organelles. First, we used HEK 293T cells co-expressing Luc-ER on top of the expression of the components of the lipid-depletion system and the PM-targeted Venus proteins. Since the ER has a large surface, we reasoned that proteins released from the PM would generate a signal with the ER-targeted luciferase. As shown on Fig. 3B upon PM PPIs depletion we did detect increased energy transfer in cells expressing the Venus-K-Ras-CAAX or c-Src₁₋₁₅-Venus constructs ($2.73 \times 10^{-2} \pm 0.723 \times 10^{-2}$ $P < 0.001$, $1.61 \times 10^{-2} \pm 0.284 \times 10^{-2}$ $P = 0.027$, resp.). There was no significant change, however, in the case of the other PM targeting sequences.

Next, we investigated whether these two targeting motifs can generate energy transfer with luciferase targeted to the surface of other organelles. As shown in Fig. 3C, releasing Venus-K-Ras-CAAX from the PM has generated a significant increase in the BRET signal in the Golgi ($9.0 \times 10^{-2} \pm 0.256 \times 10^{-2}$ $P = 0.001$) but not in early endosomes. In the case of the mitochondria we detected a very small, but still significant increase ($0.712 \times 10^{-2} \pm 0.15 \times 10^{-2}$ $P = 0.026$). c-Src₁₋₁₅-tagged Venus resulted in similar change (data not shown). Importantly, we did not detect any interaction between Golgi-Luc and Venus-H-Ras-CAAX after PM PPIs depletion (Fig. 3D).

As an important control experiment, we determined that PM PPIs depletion did affect the localization of the organelle-targeted luciferases. As shown on Fig. S1 confocal microscopy did not reveal any detectable change in the localization of the constructs (here luciferase was replaced by Cerulean).

Translocation of Venus-K-Ras-CAAX from the PM to the Golgi happens through the cytoplasm and depends on the Golgi PtdIns4P level

Previous studies have shown that rather than using vesicle trafficking the K-Ras proteins move between intracellular membranes through binding to “solubilizing factors” such as Galectin-3 and PDE δ to prevent random attachment to the endomembranes (6,25). Structural analysis, showed

that these transport proteins provide with a hydrophobic groove suitable to adopt the hydrophobic farnesyl group on the K-Ras protein, thereby increasing its water solubility (26-28). To test how this process affects the translocation of the protein from the PM to the Golgi, we pretreated cells with deltarasin, a compound that competes to Ras binding by mimicking the structure of farnesyl groups (26). Deltarasin treatment significantly reduced (from $7.47 \times 10^{-2} \pm 0.218 \times 10^{-2}$ to $3.29 \times 10^{-2} \pm 0.692 \times 10^{-2}$ $P = 0.005$) the appearance of Venus-K-Ras-CAAX at the Golgi upon PM PPIs depletion (Fig. 4A). Confocal images on Fig. 4B also show that in deltarasin pretreated COS-7 cells a reduced amount of Venus-K-Ras-CAAX reached the Golgi upon the rapamycin treatment. Instead, Venus-K-Ras-CAAX remained bound to intracellular vesicular structures. Notably, deltarasin treatment alone significantly reduced K-Ras-CAAX Golgi interaction ($-1.94 \times 10^{-2} \pm 0.374 \times 10^{-2}$ $P = 0.039$), suggesting that even in resting cells (without PM PPIs depletion) there is a rapid cycling of K-Ras-CAAX tagged proteins between the Golgi and the PM (Fig. S2A).

To confirm that Venus-K-Ras-CAAX can exist in the cytoplasm not in a membrane bound, but in free, solubilized form, we carried out a simple experiment. Cells that expressed Venus-K-Ras-CAAX were treated with the permeabilization agent digitonin allowing the release of small cytoplasmic proteins from the cell. As shown on Fig. 4D upon the permeabilization Venus-K-Ras-CAAX also appeared in the membrane of the other, non-transfected cells of the culture, supporting the hypothesis of the membrane-independent cytoplasmic trafficking. This phenomenon was never noticed when H-Ras-CAAX was used instead of the K-RAS-CAAX (Fig. 4D).

To examine whether it is the Golgi PtdIns4P that recruits the Venus-K-Ras-CAAX during its Golgi translocation, we performed BRET measurements in which in addition to depletion of PM PPIs, the PtdIns4P pool of the Golgi was also reduced. To do this, we co-transfected HEK 293T cells with plasmids that targeted FRB both to the PM and the Golgi for the rapamycin-dependent PJ translocation to both compartments (Fig. 4D). As shown on Fig. 4D upper plot, concomitant Golgi PtdIns4P depletion resulted in a significantly lower (from $3.99 \times 10^{-2} \pm 0.422 \times 10^{-2}$ to $1.81 \times 10^{-2} \pm$

0.0704×10^{-2} $P=0.007$) translocation of the K-Ras-CAAX tagged Venus, compared to the case where PPIns depletion occurred only at the PM. Control measurements of PM PtdIns(4,5) P_2 was carried out to show that the decrease of the Golgi translocation of Venus-K-Ras-CAAX was not due to a lesser PM phospholipid depletion (Fig. 4E lower plot).

PM binding of Venus-K-Ras-CAAX depends on electrostatic interactions rather than binding to specific lipids

As shown in Fig. 2, rapamycin-induced PJ-recruitment led to acute depletion of PtdIns4P, PtdIns(4,5) P_2 and PtdIns(3,4,5) P_3 in the PM. To investigate whether any of these lipids has a specific role keeping the K-Ras-CAAX-tagged Venus in the PM, we depleted these PPIns individually.

As shown in Fig. 5A, the robust PtdIns(3,4,5) P_3 depletion in the PM achieved by Wm treatment (see Fig. 2C) did not cause Venus-K-Ras-CAAX to appear in the Golgi compartment, nor did it affect the Golgi translocation response following PJ recruitment to the PM. This suggests that PM PtdIns(3,4,5) P_3 plays a negligible role in the stabilization of the Venus-K-Ras-CAAX protein at the PM.

Next, we depleted PM PtdIns4P and PtdIns(4,5) P_2 separately to examine the contribution of these lipids individually to the PM localization of the K-Ras. For this, we used PJ enzymes inactivated in either its 5-phosphatase (FKBP-PJ-4ptase) or 4-phosphatase (FKBP-PJ-5ptase) activities (15). As shown in Fig. 5B, FKBP-PJ-5ptase recruitment, which reduced only the PM PtdIns(4,5) P_2 level (with a slight increase in PM PtdIns4P), caused an about 40% reduction (from $7.67 \times 10^{-2} \pm 0.71 \times 10^{-2}$ to $4.58 \times 10^{-2} \pm 1.21 \times 10^{-2}$ $P=0.00287$) of Venus-K-Ras-CAAX translocation to the Golgi when compared to the effect of FKBP-PJ. Recruitment of the FKBP-PJ-4ptase, which reduced only PM PtdIns4P was less effective (85% reduction), but still caused a significant increase ($1.25 \times 10^{-2} \pm 0.041 \times 10^{-2}$ $P=0.003$) of K-Ras-CAAX Golgi appearance (Fig. 5B).

The effect of PM PPIns depletion on the intracellular trafficking of full-length K- and H-Ras proteins

In the previous experiments, we examined the isolated targeting sequences of the Ras proteins. To

study the behavior of the full-length Ras proteins, we created N-terminally Venus-tagged versions of the full-length K- and H-Ras proteins, and investigated their movements under conditions of PPIns manipulations. In these experiments, the constitutively active forms G12V of both Ras proteins were used. As shown on Fig. 6, the full-length proteins showed the same changes in response to PPIns depletion as their isolated targeting sequences examined both by confocal microscopy (Fig. 6A) and BRET (Fig. 6B and C) in HEK 293T cells ($1.34 \times 10^{-2} \pm 0.275 \times 10^{-2}$ $P=0.049$, $3.56 \times 10^{-2} \pm 0.567 \times 10^{-2}$ $P=0.02$, resp.). Wild type or dominant negative forms of the Ras proteins, behaved the same way indicating that the translocation process is independent of the activity state of these proteins (Fig. S3).

K-Ras moves to the Golgi during G_q-coupled or EGF receptor activation

After testing Ras distribution using the artificial PPIns manipulations, we wanted to determine how PPIns changes that occur during more physiological conditions, namely during G_q-coupled receptor activation affect the intracellular distribution of the K-Ras protein. For this, M3 muscarinic receptors (M3R) were expressed in HEK 293T cells, together with either Venus-K-Ras-CAAX or Venus-K-Ras G12V constructs and the Golgi-Luc protein to examine K-Ras translocation to the Golgi membrane in BRET measurements. The M3R agonist, carbachol was used to stimulate PLC activation. Distribution of the Venus-K-Ras-CAAX construct was also examined with confocal microscopy, using transiently transfected COS-7 cells. As shown in Fig. 7A, carbachol treatment caused a moderate transient elevation in the Golgi appearance of either Venus-K-Ras-CAAX or the full Venus-K-Ras G12V protein ($1.28 \times 10^{-2} \pm 0.0521 \times 10^{-2}$ $P=0.013$, $0.759 \times 10^{-2} \pm 0.106 \times 10^{-2}$ $P=0.005$, resp.), which was more pronounced with the Venus-K-Ras-CAAX construct. Pretreatment of the cells with A1, an inhibitor of the type-III PI4K α kinase (PI4KA), which prevents PtdIns4P and PtdIns(4,5) P_2 resynthesis, resulted in a more sustained effects. Similar changes were observed in COS-7 cells using confocal microscopy (Fig. 7B). Notably, A1 treatment increased K-Ras-CAAX Golgi interaction ($1.56 \times 10^{-2} \pm 0.167 \times 10^{-2}$ $P=0.049$), suggesting that even in resting cells PM PtdIns4P

depletion alone can evoke translocation of K-Ras-CAAX to the Golgi (Fig. S2B).

Previously we showed that stimulation of HEK 293T cells with EGF decreases PM PtdIns(4,5) P_2 level by activating the generation of PtdIns(3,4,5) P_3 and IP3 by PI3 kinases and PLC γ , respectively (24). Interestingly the latter effect could not be abolished by low concentration of Wm (100 nM) (24). To examine whether this decrease of PM PtdIns(4,5) P_2 can have an impact on the distribution of K-Ras, we decided to measure arrival of the Venus-K-Ras-CAAX to the Golgi. Stimulation of endogenous EGF receptors of HEK cells by 100 ng/ml EGF failed to cause a detectable translocation from the PM to the Golgi (data not shown). However, when cells were co-transfected with the EGF receptor, EGF stimulation caused translocation of Venus-K-Ras-CAAX from the PM to the Golgi in a similar way, as did M3R stimulation ($0.665 \times 10^{-2} \pm 0.293 \times 10^{-2}$ $P=0.002$) (Fig. 7C). Similarly, this effect was even larger when PI4KA was inhibited with A1 consistent with the notion that depletion of plasma membrane PtdIns4P and PtdIns(4,5) P_2 together liberates K-Ras, which is then recruited to the Golgi by PtdIns4P in that compartment (Fig. 7C). In contrast, inhibition and subsequent depletion of the PM PtdIns(3,4,5) P_3 did not enhance the translocation (Fig. 7C), which is also consistent with its minor effect on the PM recruitment of K-Ras (Fig. 5A).

PM PPIs depletion attenuates K-Ras but not H-Ras induced cell proliferation

Ras proteins control numerous cellular processes ranging from cell growth to differentiation and cell survival (29). To investigate the functional consequences of K-Ras translocation to the Golgi after PM PPIs depletion, we carried out a 24 hour [3 H]-Leucine incorporation assay to evaluate the rate of the protein synthesis as marker of cell proliferation.

First, the proliferative effect of the constitutive active mutation of Ras was examined. Constitutive active G12V and dominant negative S17N forms of the K- and H-Ras proteins were expressed transiently in COS-7 cells. As expected, cells expressing the activating Ras mutants showed significantly larger Leucine incorporation compared to those expressing the dominant negative forms ($P<0.001$) (Fig. 8A). This increased protein synthesis was used as a sign of increased

proliferation caused by the active Ras mutants. Next, we examined how the PM PPIs depletion affects the ability of active Ras to induce proliferation. Again, PM PPIs depletion was achieved using recruitment of FKBP-PJ. Since rapamycin, an mTOR inhibitor was used for recruitment; we used the catalytically inactivated FKBP-PJ enzyme as control (15). As shown on Fig. 8B, active K-Ras increased the [3 H]-Leucine incorporation even in the presence of 100 nM rapamycin, although its effect was reduced (compare Fig. 8A and B). PM PPIs depletion did not affect the already low [3 H]-Leucine incorporation in cells expressing the dominant negative form of K-Ras S17N, but had a significant inhibitory effect ($P=0.003$) in cells expressing the active form of K-Ras G12V. Notably, PPIs depletion did not change the proliferative effect of H-Ras G12V. This was in agreement with the earlier data showing that H-Ras G12V PM localization does not depend on the PM PPIs. These experiments showed that only the PM-localized Ras is competent in signaling to proliferation and the Golgi-associated form is unable to induce the same changes under PPIs-depleted conditions.

Discussion

PM localization plays a fundamental role in the function of many intracellular signaling proteins. Several factors determine PM localization of a protein, some of which are intrinsic to the protein, such as the presence of hydrophobic lipid modifications or transmembrane segments. Some of the interactions, however, rely upon specific lipid components of the membrane, such as PPIs or simple electrostatic interactions provided by acidic lipids, such as PtdSer. In this study, we investigated how depletion of negatively charged PPIs can acutely regulate the PM association and intracellular distribution of selected peripheral PM proteins. We focused on two members of the Ras family, K-Ras and H-Ras. The C-terminus of both of these proteins undergo prenylation, but this alone is not sufficient for stable PM interaction. In the case of K-Ras electrostatic interactions between positively charged residues located within the C-terminal tail of the molecule and negatively charged phospholipids of the PM is required for PM

localization. In contrast, H-Ras, has two additional palmitoylations in its C-terminus that ensures PM localization. These features have major impact on the different signaling properties of these Ras proteins (30,31).

In this study we used an adaptation of our recently developed BRET system to have a more quantitative assessment of the role of the individual PPIs on K-Ras and H-Ras PM localization. Moreover, we also developed a method to have a quantitative assessment of which intracellular membranes Ras molecules will interact with once released from the PM. We combined these BRET measurements with the controlled elimination of PtdIns4P and PtdIns(4,5)P₂ using the rapamycin-inducible membrane recruitment of the bifunctional artificial PPIs phosphatase, pseudojanin (PJ) (15). Using this system, we confirmed previous findings (13-15) that both PtdIns4P and PtdIns(4,5)P₂ were important for PM localization of K-Ras, but PtdIns(4,5)P₂ was more important, and PtdIns(3,4,5)P₃ played little if any roles. This discrepancy could be explained with the generation of stronger local electric field by PtdIns(4,5)P₂, especially, if it is present in clusters in the PM (32-34), or it is caused by the insufficient PM PtdIns4P depletion when PJ-4ptase is used instead of PJ (compare PM PtdIns4P measurement on Fig2C and Fig 5B). Recently, based on the ability to form long-lived salt bridges the distinguished role of PtdIns(4,5)P₂ was also shown (35).

Although PPIs appear to be the most important in K-Ras PM recruitment, the role of PtdSer on K-Ras localization has been reported (36-39). Although PS only carries a single negative charge it is present in the inner leaflet of the PM in relatively high amount (34), therefore, could contribute to the localization of proteins containing basic surface patches. Indeed, it was found that by decreasing the PM PtdSer level (measured by LactC2 (12)), 7-oxostaurosporine or fendiline could effectively reduce the amount of the PM bound K-Ras in MDCK cells (36,37,39). Unfortunately, a long-term exposure (at least 24-hour) to these inhibitors was required to achieve the lipid change and several other changes could occur during this treatment regime. Our effort to acutely reduce PM PtdSer has not been successful so far and therefore we could not assess the role of PS in K-Ras PM localization. These efforts are still being continued in our laboratory.

An important new aspect of our study was to follow the fate of the K-Ras protein once it was released from the PM during PPIs depletion. Again, using a BRET analysis that monitors the appearance of the K-Ras protein in membranes of the ER, Golgi, endosomes or mitochondria, we showed that K-Ras rapidly appears in the Golgi and to a smaller extent in the ER, but not in the endosomes after being released from the PM. In case of the mitochondria there is a slight increase of the energy transfer between the mitochondria-targeted luciferase and the Venus-K-Ras-CAAX, but it is negligible compared to the Golgi, and reflects the appearance of the Venus in the cytoplasm. According to the current views, after released from the PM K-Ras binds transport proteins such as Galectin-3 and PDE δ that keep it in the cytosol. Our results are consistent with this idea since the Golgi translocation of the Venus-K-Ras-CAAX protein was prevented by treatment with deltarasine, a compound that mimics the farnesyl groups and competes for K-Ras binding of the transport molecules. Moreover, Venus-K-Ras-CAAX can leave the cytoplasm when cells are permeabilized. Interestingly, when the cytoplasmic transport is inhibited Venus-K-Ras-CAAX appears on the surface of intracellular vesicles, probably because they are negatively charged by PtdIns3P and close to the PM, therefore, are able to trap Venus-K-Ras-CAAX. Since the electrostatic interaction seems to be major determinant of the membrane binding even in case of endomembranes, it is not surprising that PtdIns4P depletion of Golgi does also not favor the localization of the proteins in the Golgi.

Could there be a physiological significance of the Golgi localization of K-Ras? There are many examples in the literature that small G-proteins proteins are capable of initiating signaling events from endomembranes, including the Golgi. It has been reported that Ras proteins can be activated at the Golgi (40,41), and are able to initiate proliferation signals through the activation of ERK (42). These reports, however, referred to H- and N-Ras, but not K-Ras4B, since during its intracellular trafficking K-Ras is not found in the Golgi (6). However, a potential significance of the translocation of K-Ras from the PM to the endomembranes including ER and Golgi could be that Ras signaling might be switched on in these other localizations, if RasGRPs can control their

activation state (43,44). Bivona et al described the PKC-dependent translocation of K-Ras from the PM to endomembranes including the Golgi and the mitochondria by a mechanism, which included the phosphorylation of serine residues on the C-terminal tail of K-Ras, disrupting the electrostatic interaction between the protein and the membrane (45). However, we could not detect the appearance of Venus-K-Ras-CAAX either in the Golgi or in the mitochondria upon PMA treatment. This apparent discrepancy could be explained with the different stimulation regime in the Bivona studies and ours; to activate PKC they used bryostatin and since PMA alone was found to be ineffective, they also added ionomycin, which by increasing Ca^{2+} could have evoked PPIs depletion.

The proliferating effect of the Ras proteins depends on the activation of three distinct pathways: 1.) active Ras can elevate PM $\text{PtdIns}(3,4,5)\text{P}_3$ levels due to activation of PI3K enzymes and therefore activates Akt signaling 2.) it can directly activate the MAPK cascade via activation of Raf proteins and 3.) it can activate the Ral-GDS protein, which then triggers the conversion of GDP bound inactive Ral proteins to GTP bound active form (3). Although this latter pathway is less established compared to the plenty of literature on the first two pathways, its significance is increasing as a major factor in the transforming ability of the Ras proteins (31,46). We used the 24 hour [^3H]-Leucine incorporation as a measure of Ras-induced proliferation after expression of the various Ras proteins either in their active G12V or inactive S17N forms. To test the effect of PPIs depletion on Ras signaling we used the rapamycin-recruitable PJ enzyme. These experiments showed that K-Ras but not H-Ras signaling (as it translates to [^3H]-Leucine incorporation) was highly dependent on PM PPIs suggesting that it is the PM-bound form that is important for signaling and increased Golgi association does not support a proliferative effect. Importantly in cells that expressed oncogenic Ras, [^3H]-Leucine incorporation was increased even in the presence of 100 nM rapamycin, which inhibits mTOR signaling (47,48). In contrast to K-Ras, the increased proliferation evoked by H-Ras expression did not depend on PM PPIs (including $\text{PtdIns}(3,4,5)\text{P}_3$). This finding was somewhat unexpected in light of numerous reports showing that PPIs are required for the normal function of

several members of the MAPK pathway (49,50). We also found that ERK phosphorylation was reduced by PM PPIs depletion (G. Gulyás and P. Várnai unpublished observations) raising the possibility that the proliferative effects of K-Ras are mediated primarily by the Ral pathway. Although there is a paper suggesting that the Ral pathway is originated from the Golgi (51), it is widely accepted that active PM-bound Ras proteins can activate cell proliferation through the Ral-TBK1 pathway (52). Additionally, we can find examples in the literature that palmitoylation could also occurs on further cysteine residues away from the terminal cysteine within the C-terminal tail domain, which strengthen the PM anchoring of Ral, and prevent the detachment of this molecule from the PM after PM PPIs depletion, as could be seen in the case of the H-Ras protein (53,54).

Lastly, there is a plethora of literature concerning the segregation of the various PM targeting sequences in lateral domains of the PM often referred to as rafts (16,55). However, there is a significant amount of controversy surrounding this topic (56,57). CAAX domains with polybasic residues are often used to target domains outside of rafts, whereas the Lyn domain is used to target rafts (58). Notably, however, it was suggested that $\text{PtdIns}(4,5)\text{P}_2$ is found in rafts (59), which is where CAAX domains with polybasic sequences would be enriched. The distribution of $\text{PtdIns}(4,5)\text{P}_2$ or its protein binding partners to specialized PM domains could not be substantiated by several credible efforts (60,61). This topic is worth mentioning because of the significant literature on the distribution of the various Ras proteins into specialized PM domains designated as rafts (62-64). Unfortunately, our studies were unable to shed any light on this topic and several efforts in our group failed to detect a difference between the ability of any of these PM targeting sequences to access PPIs when used to recruit PPIs modifying enzymes (P. Várnai, G. Gulyás and T Balla unpublished observations).

In summary, these studies were aimed at assessing the role of PM PPIs in the localization of various PM targeting sequences using a BRET-based method for quantitative assessment. In agreement with the literature, we found that sequences that use polybasic stretches in addition to lipid modifications depend on PPIs for membrane attachment by principle of electrostatic interactions

rather than specific PPIs binding. Using the K-Ras protein as an example, we also followed the intracellular fate of the protein and showed that it associated with the Golgi in a PtdIns4P-dependent manner once released from the PM, but this Golgi-associated pool was unable to maintain the proliferative effect of the K-Ras protein.

Experimental procedures

Materials

Molecular biology reagents were purchased from Fermentas (Vilnius, Lithuania). For the polymerase chain reaction, the Pfu Turbo Hotstart polymerase was used (Agilent Technologies; Santa Clara, CA). Cell culture dishes, 24- and 96-well plates were obtained from Greiner (Kremsmunster, Austria). 8-well μ -Slides (Cat. No.: 80826) for confocal experiments were obtained from IBIDI (Martinsried, Germany). Coelenterazine h was purchased from Regis Technologies (Morton Grove, IL). Lipofectamine 2000 was from Invitrogen (Carlsbad, CA). Rapamycin and PIK-93 were obtained from Selleckchem (Houston, TX). GeneCellin transfection reagent was from BioCellChallenge (Toulon, France). Deltarazine was purchased from Cayman Chemicals (Ann Arbor, MI). Unless otherwise stated, all other chemicals and reagents were purchased from Sigma (St Louis, MO).

DNA constructs

To create the various PM targeted Venus constructs, the targeting sequences of the following proteins were synthesized: the N-terminal 14 amino acids (AA) of Lyn (Lyn₁₋₁₄, accession number: NM_002350.3), the N-terminal 10 AA of Lck (Lck₁₋₁₀, accession number: NM_005356.4), the N-terminal 15 AA of c-Src (c-Src₁₋₁₅, accession number: NM_005417.4), and the C-terminal 22 AA both of K-Ras4B, and H-Ras proteins (K-Ras-CAAX, accession number: NM_004985; H-Ras-CAAX, accession number: NM_005343, respectively). The fragments were then inserted into monomeric Venus (containing the A206K mutation (16)) encoding N1 vector using the NheI and BglII enzymes in the case of the N-terminal targeting sequences, or into C1 plasmid using the EcoRI and BamHI sites in the case of the C-terminal Ras sequences. The following linkers were

applied by these constructs: DPTRSRAQASNSDPPVAT in the case of the Lyn₁₋₁₄-Venus, NNNNDPTRSRAQASNSDPPVAT was used both by Lck₁₋₁₀-Venus and c-Src₁₋₁₅-Venus (17), and NEQRSRAQASNS in the case of the Ras constructs. The fluorescent Citrine tagged full-length K-Ras4B G12V (accession number: NM_004985) and the wild type or G12V mutant H-Ras (accession number: NM_005343) encoding plasmids were a kind gift from John F Hancock. To create our monomeric Venus tagged versions, the sequences of the Ras proteins were amplified using PCR, and the fragments were cloned into monomeric Venus containing C1 vectors using the YSDLELTTMYPYDVPDYA linker in both proteins. The missing mutant versions of the Ras proteins (K-Ras wt, K-Ras S17N, and H-Ras S17N) were created using site directed mutagenesis.

To create the various endomembrane targeted Luciferase constructs, the targeting sequences or the full-length forms of the following proteins were used: TOM70 (accession number: X05585.1), TGN38 (accession number: BC008461), Sac1 (accession number: NM_001179777) and EEA (Fyve domain; accession number: BX648463) for mitochondria, Golgi, endoplasmic reticulum and early endosome targeting, respectively. The N-terminal coding sequence of the first 30 AA of the TOM-70 protein was synthesized, and then was ligated into super Renilla luciferase (65) containing N1 plasmid, using the NheI and BglII enzyme pairs. The sequences of the TGN38 (66), Sac1 (67) or EEA1 (68) were used earlier. The proper fragments of these proteins were amplified with polymerase chain reaction, then were inserted into super Renilla Luciferase containing N1 vector using NheI and BglII enzymes in the case of the TGN38-Luciferase construct or into super Renilla Luciferase containing C1 vector using EcoRI and BamHI sites by Luc-ER and Luciferase-EEA1-FYVE constructs. The following linkers were applied by these constructs: DPTRSRAQASNSDPPVAT was used both by TOM70 and TGN38, whereas the SGLRSRAQASNSRV and the RSRAQASNSRV sequence was used in the case of the Luciferase-Sac1 and Luciferase-EEA1-FYVE proteins, respectively.

The rapamycin inducible lipid depletion system, applied for the PM PPIs depletion (24),

and the TGN38-FRB-mRFP, which were used for recruiting our cytoplasmic phosphatase to the Golgi (66), were described earlier. The specific BRET-based lipid-sensors and the fluorescently tagged versions of either SidM-2x-P4M or PLC δ 1-PH constructs or luciferase tagged versions of the PLC δ 1-PH domain were also previously used (24).

Wild type human M3 cholinergic receptor (N-terminal 3x-hemagglutinin tagged) was obtained from S&T cDNA Resource Center (Rolla, MO). The human EGF receptor was described earlier (24).

Cell culture

HEK 293T and COS-7 cells (ATCC, Manassas, VA) were maintained in Dulbecco's modified Eagle's medium (DMEM, Lonza 12-604) supplemented with 10% fetal bovine serum, 50 U/ml penicillin and 50 μ g/ml streptomycin in a 5% humidified CO₂ incubator at 37°C in 10 cm tissue culture plastic dishes.

Bioluminescence Resonance Energy Transfer (BRET) measurements

For BRET measurements HEK 293T cells were trypsinized and plated on poly-L-lysine-pretreated (0.001%, 1 hour) white 96-well plates at a density of 7×10^4 cells/well together with the indicated DNA constructs (0.15-0.2 μ g total DNA/well) and the cell transfection reagent (1.5 μ l/well GeneCellin) in Opti-MEM reduced serum medium (Gibco). After 6 hours 100 μ l/well DMEM containing serum and antibiotics was added. Measurements were performed 25-26 hours after transfection. Before the measurements, the medium over the cells was changed to a medium (50 μ l) containing 120 mM NaCl, 4.7 mM KCl, 1.2 mM CaCl₂, 0.7 mM MgSO₄, 10 mM glucose, and 10 mM Na-HEPES, pH 7.4. Measurements were performed at 37°C using a Thermoscientific Varioskan Flash Reader (PerkinElmer). The measurements started with the addition of the cell permeable luciferase substrate, coelenterazine h (40 μ l, final concentration of 5 μ M), and counts were recorded using 485 and 530 nm emission filters. Detection time was 500 ms for each wavelength. The indicated reagents were also dissolved in modified Krebs-Ringer buffer and were added manually in 10 μ l. For this, plates were unloaded, which resulted in an interruption in the recordings. All measurements were done in 2-4 biological replicates. By the measurements of the

PM lipid levels, BRET ratios were calculated by dividing the 530 nm and 485 nm intensities, and normalized to the baseline. Since the absolute ratio values depended on the expression of the sensors in case of the intermolecular inositol lipid sensors the resting levels were considered as 100%, whereas the 0% was determined from values of those experiments where cytoplasmic *Renilla* luciferase construct was expressed alone. In the case of the interaction experiments between the Venus tagged PM-targeted constructs and Luciferase tagged endomembrane targeted constructs, the difference of the BRET ratios was calculated between rapamycin (300 nM) or carbachol (10 μ M) treated and vehicle (DMSO, or distilled water) treated cells, respectively.

Confocal microscopy

HEK 293T cells at a density of 3×10^4 cells/well or COS-7 cells at a density of 2×10^4 cells/well were cultured on IBIDI 8 well μ Slides in Dulbecco's modified Eagle's medium (DMEM, Lonza 12-604) supplemented with 10% fetal bovine serum, 50 U/ml penicillin and 50 μ g/ml streptomycin at 37°C. After one day, the culture medium was changed to 200 μ l transfection solution containing the indicated DNA constructs (0.2 μ g total DNA/well) and 0.33 μ l/dish Lipofectamine 2000. After 6 hours, the transfection solution was changed to 300 μ l supplemented DMEM culture medium. Confocal measurements were performed 24-26 hours after transfection at room temperature in a modified Krebs-Ringer buffer described above, using a Zeiss LSM 710 scanning confocal microscope and a 63x/1.4 oil-immersion objective. Post-acquisition picture analysis was performed using Fiji and Photoshop (Adobe) software's to expand to the full dynamic range but only linear changes were allowed.

Permeabilization measurements

HeLa cells were cultured on 25 mm No. 1.5 glass coverslips (2×10^5 cells/dish) and transfected with Venus-K-Ras-CAAX or Venus-H-Ras-CAAX constructs (0.5 μ g DNA/dish) using 2 μ l/dish Lipofectamine 2000 for 24 h. Confocal measurements were performed at room temperature in an intracellular medium containing 117 mM KCl, 6 mM NaCl, 1 mM KH₂PO₄, 10 mM K⁺-MOPS, 2 mM EGTA, 0.5 mM MgCl₂ and 100 nM CaCl₂, pH 7.1; using a Zeiss LSM 710 confocal microscope

and a 63x/1.4 oil-immersion objective. For the permeabilization 25 µg/ml digitonin was applied.

[³H]-Leucine incorporation assay

The effect of PM lipid depletion on protein synthesis in COS-7 cells was evaluated by a [³H]-Leucine incorporation assay. 5×10⁴ cells were seeded in poly-L-lysine-pretreated (0.001%, 1 hour) 24-well plates and left to adhere overnight at 37°C. The cells transfected with plasmids and after 1 day the cells were incubated with serum-free DMEM for 6 hours. The quiescent COS-7 cells were further incubated in serum-free DMEM containing 1 µCi/ml [³H]-Leucine (American Radiolabeled Chemicals, Saint Louis, MO, USA) with or without 100 nM rapamycin (repeated in every 8 hours). After 24 hours of incubation the plates were placed on ice, the cells were washed twice with ice-cold PBS, and incubated for 30 min in cold trichloroacetic acid (5%). The fixed cells were then washed with PBS and dissolved in 0.5 M NaOH for 30 min. Finally, the lysed cells were transferred to scintillation vials containing 10 ml of OptiPhase HiSafe3 (Perkin Elmer, Waltham, MA,

USA). The radioactivity was counted by Beckman LS5000 TD liquid scintillation counter.

Statistical analysis

For the statistical analysis of ΔBRET ratio data, paired t-test was used to compare the mean of the last three data points before and after the stimulation of the individual curves. When two separate curves were compared, unpaired t-test was also performed on the means of the last three data points of the curves after the stimulation. When three separate curves were compared, one-way ANOVA was used followed by Holm-Sidak all pairwise multiple comparison method on the means of the last three data points of the curves after the stimulation. To investigate the effects of the different Ras mutants and/or the PM PPIs depletion system in the [³H]-Leucine incorporation assay, two-way ANOVA followed by Holm-Sidak all pairwise multiple comparison method was used. Statistical analysis was performed using SigmaStat 3.5 program (Systat Software Inc., San Jose, CA, USA).

Acknowledgement: PV was supported by the National Research, Development and Innovation Fund (NKFIH K105006). TB was supported by the Intramural Research Program of the Eunice Kennedy Shriver National Institute of Child Health and Human Development of the National Institutes of Health. The technical assistance of Kata Szabolcsi is highly appreciated. The content is solely the responsibility of the authors and does not necessarily represent the official views of the National Institutes of Health.

Conflict of interest: The authors declare that they have no conflicts of interest with the contents of this article.

Author contributions: GG designed and constructed vectors, designed, performed and analyzed the experiments, contributed to the preparation of the figures and wrote the paper. GR designed, performed and analyzed the experiments. RM performed experiments. AB designed, performed and analyzed the experiments shown in Figures 8. LH conceived and coordinated the study. TB analyzed the experiments and wrote the paper. PV conceived and coordinated the study, designed and constructed vectors, designed, and analyzed the experiments contributed to the preparation of the figures and wrote the papers. All authors analyzed the results and approved the final version of the manuscript.

References

1. Whited, A. M., and Johs, A. (2015) The interactions of peripheral membrane proteins with biological membranes. *Chem Phys Lipids* **192**, 51-59
2. Wennerberg, K., Rossman, K. L., and Der, C. J. (2005) The Ras superfamily at a glance. *J Cell Sci* **118**, 843-846
3. Lu, S., Jang, H., Muratcioglu, S., Gursoy, A., Keskin, O., Nussinov, R., and Zhang, J. (2016) Ras Conformational Ensembles, Allostery, and Signaling. *Chem Rev* **116**, 6607-6665
4. Prior, I. A., Lewis, P. D., and Mattos, C. (2012) A comprehensive survey of Ras mutations in cancer. *Cancer Res* **72**, 2457-2467
5. Rocks, O., Peyker, A., Kahms, M., Verveer, P. J., Koerner, C., Lumbierres, M., Kuhlmann, J., Waldmann, H., Wittinghofer, A., and Bastiaens, P. I. (2005) An acylation cycle regulates localization and activity of palmitoylated Ras isoforms. *Science* **307**, 1746-1752
6. Wright, L. P., and Philips, M. R. (2006) Thematic review series: lipid posttranslational modifications. CAAX modification and membrane targeting of Ras. *J Lipid Res* **47**, 883-891
7. Silvius, J. R., Bhagatji, P., Leventis, R., and Terrone, D. (2006) K-ras4B and prenylated proteins lacking "second signals" associate dynamically with cellular membranes. *Mol Biol Cell* **17**, 192-202
8. Choy, E., Chiu, V. K., Silletti, J., Feoktistov, M., Morimoto, T., Michaelson, D., Ivanov, I. E., and Philips, M. R. (1999) Endomembrane trafficking of ras: the CAAX motif targets proteins to the ER and Golgi. *Cell* **98**, 69-80
9. Scheidt, H. A., and Huster, D. (2009) Structure and dynamics of the myristoyl lipid modification of SRC peptides determined by 2H solid-state NMR spectroscopy. *Biophys J* **96**, 3663-3672
10. Kay, J. G., Koivusalo, M., Ma, X., Wohland, T., and Grinstein, S. (2012) Phosphatidylserine dynamics in cellular membranes. *Mol Biol Cell* **23**, 2198-2212
11. Stahelin, R. V., Scott, J. L., and Frick, C. T. (2014) Cellular and molecular interactions of phosphoinositides and peripheral proteins. *Chem Phys Lipids* **182**, 3-18
12. Yeung, T., Gilbert, G. E., Shi, J., Silvius, J., Kapus, A., and Grinstein, S. (2008) Membrane phosphatidylserine regulates surface charge and protein localization. *Science* **319**, 210-213
13. Yeung, T., Terebiznik, M., Yu, L., Silvius, J., Abidi, W. M., Philips, M., Levine, T., Kapus, A., and Grinstein, S. (2006) Receptor activation alters inner surface potential during phagocytosis. *Science* **313**, 347-351
14. Heo, W. D., Inoue, T., Park, W. S., Kim, M. L., Park, B. O., Wandless, T. J., and Meyer, T. (2006) PI(3,4,5)P3 and PI(4,5)P2 lipids target proteins with polybasic clusters to the plasma membrane. *Science* **314**, 1458-1461
15. Hammond, G. R., Fischer, M. J., Anderson, K. E., Holdich, J., Koteci, A., Balla, T., and Irvine, R. F. (2012) PI4P and PI(4,5)P2 are essential but independent lipid determinants of membrane identity. *Science* **337**, 727-730
16. Zacharias, D. A., Violin, J. D., Newton, A. C., and Tsien, R. Y. (2002) Partitioning of lipid-modified monomeric GFPs into membrane microdomains of live cells. *Science* **296**, 913-916
17. Johnson, C. M., Chichili, G. R., and Rodgers, W. (2008) Compartmentalization of phosphatidylinositol 4,5-bisphosphate signaling evidenced using targeted phosphatases. *J Biol Chem* **283**, 29920-29928
18. Toth, D. J., Toth, J. T., Gulyas, G., Balla, A., Balla, T., Hunyady, L., and Varnai, P. (2012) Acute depletion of plasma membrane phosphatidylinositol 4,5-bisphosphate impairs specific steps in endocytosis of the G-protein-coupled receptor. *J Cell Sci* **125**, 2185-2197
19. Szakadati, G., Toth, A. D., Olah, I., Erdelyi, L. S., Balla, T., Varnai, P., Hunyady, L., and Balla, A. (2015) Investigation of the fate of type I angiotensin receptor after biased activation. *Mol Pharmacol* **87**, 972-981

20. Varnai, P., Thyagarajan, B., Rohacs, T., and Balla, T. (2006) Rapidly inducible changes in phosphatidylinositol 4,5-bisphosphate levels influence multiple regulatory functions of the lipid in intact living cells. *J Cell Biol* **175**, 377-382
21. Hammond, G. R., Machner, M. P., and Balla, T. (2014) A novel probe for phosphatidylinositol 4-phosphate reveals multiple pools beyond the Golgi. *J Cell Biol* **205**, 113-126
22. Varnai, P., and Balla, T. (1998) Visualization of phosphoinositides that bind pleckstrin homology domains: calcium- and agonist-induced dynamic changes and relationship to myo-[3H]inositol-labeled phosphoinositide pools. *J Cell Biol* **143**, 501-510
23. Varnai, P., Rother, K. I., and Balla, T. (1999) Phosphatidylinositol 3-kinase-dependent membrane association of the Bruton's tyrosine kinase pleckstrin homology domain visualized in single living cells. *J Biol Chem* **274**, 10983-10989
24. Toth, J. T., Gulyas, G., Toth, D. J., Balla, A., Hammond, G. R., Hunyady, L., Balla, T., and Varnai, P. (2016) BRET-monitoring of the dynamic changes of inositol lipid pools in living cells reveals a PKC-dependent PtdIns4P increase upon EGF and M3 receptor activation. *Biochim Biophys Acta* **1861**, 177-187
25. Elad-Sfadia, G., Haklai, R., Balan, E., and Kloog, Y. (2004) Galectin-3 augments K-Ras activation and triggers a Ras signal that attenuates ERK but not phosphoinositide 3-kinase activity. *J Biol Chem* **279**, 34922-34930
26. Zimmermann, G., Papke, B., Ismail, S., Vartak, N., Chandra, A., Hoffmann, M., Hahn, S. A., Triola, G., Wittinghofer, A., Bastiaens, P. I., and Waldmann, H. (2013) Small molecule inhibition of the KRAS-PDEdelta interaction impairs oncogenic KRAS signalling. *Nature* **497**, 638-642
27. Papke, B., Murarka, S., Vogel, H. A., Martin-Gago, P., Kovacevic, M., Truxius, D. C., Fansa, E. K., Ismail, S., Zimmermann, G., Heinelt, K., Schultz-Fademrecht, C., Al Saabi, A., Baumann, M., Nussbaumer, P., Wittinghofer, A., Waldmann, H., and Bastiaens, P. I. (2016) Identification of pyrazolopyridazinones as PDEdelta inhibitors. *Nat Commun* **7**, 11360
28. Schmick, M., Vartak, N., Papke, B., Kovacevic, M., Truxius, D. C., Rossmannek, L., and Bastiaens, P. I. (2014) KRas localizes to the plasma membrane by spatial cycles of solubilization, trapping and vesicular transport. *Cell* **157**, 459-471
29. Bar-Sagi, D., and Hall, A. (2000) Ras and Rho GTPases: a family reunion. *Cell* **103**, 227-238
30. Zhou, Y., and Hancock, J. F. (2015) Ras nanoclusters: Versatile lipid-based signaling platforms. *Biochim Biophys Acta* **1853**, 841-849
31. Goldfinger, L. E., and Michael, J. V. (2017) Regulation of Ras signaling and function by plasma membrane microdomains. *Biosci Trends* **11**, 23-40
32. McLaughlin, S., and Murray, D. (2005) Plasma membrane phosphoinositide organization by protein electrostatics. *Nature* **438**, 605-611
33. Fujita, A., Cheng, J., Tauchi-Sato, K., Takenawa, T., and Fujimoto, T. (2009) A distinct pool of phosphatidylinositol 4,5-bisphosphate in caveolae revealed by a nanoscale labeling technique. *Proc Natl Acad Sci U S A* **106**, 9256-9261
34. Bigay, J., and Antonny, B. (2012) Curvature, lipid packing, and electrostatics of membrane organelles: defining cellular territories in determining specificity. *Dev Cell* **23**, 886-895
35. Gregory, M. C., McLean, M. A., and Sligar, S. G. (2017) Interaction of KRas4b with anionic membranes: A special role for PIP2. *Biochem Biophys Res Commun* **487**, 351-355
36. Cho, K. J., Park, J. H., Piggott, A. M., Salim, A. A., Gorfe, A. A., Parton, R. G., Capon, R. J., Lacey, E., and Hancock, J. F. (2012) Staurosporines disrupt phosphatidylserine trafficking and mislocalize Ras proteins. *J Biol Chem* **287**, 43573-43584
37. van der Hoeven, D., Cho, K. J., Ma, X., Chigurupati, S., Parton, R. G., and Hancock, J. F. (2013) Fendiline inhibits K-Ras plasma membrane localization and blocks K-Ras signal transmission. *Mol Cell Biol* **33**, 237-251
38. Gelabert-Baldrich, M., Soriano-Castell, D., Calvo, M., Lu, A., Vina-Vilaseca, A., Rentero, C., Pol, A., Grinstein, S., Enrich, C., and Tebar, F. (2014) Dynamics of KRas on endosomes: involvement of acidic phospholipids in its association. *FASEB J* **28**, 3023-3037

39. Cho, K. J., van der Hoeven, D., Zhou, Y., Maekawa, M., Ma, X., Chen, W., Fairn, G. D., and Hancock, J. F. (2015) Inhibition of Acid Sphingomyelinase Depletes Cellular Phosphatidylserine and Mislocalizes K-Ras from the Plasma Membrane. *Mol Cell Biol* **36**, 363-374
40. Chiu, V. K., Bivona, T., Hach, A., Sajous, J. B., Silletti, J., Wiener, H., Johnson, R. L., 2nd, Cox, A. D., and Philips, M. R. (2002) Ras signalling on the endoplasmic reticulum and the Golgi. *Nat Cell Biol* **4**, 343-350
41. Balla, A., Erdelyi, L. S., Soltesz-Katona, E., Balla, T., Varnai, P., and Hunyady, L. (2011) Demonstration of angiotensin II-induced Ras activation in the trans-Golgi network and endoplasmic reticulum using bioluminescence resonance energy transfer-based biosensors. *J Biol Chem* **286**, 5319-5327
42. Jin, T., Ding, Q., Huang, H., Xu, D., Jiang, Y., Zhou, B., Li, Z., Jiang, X., He, J., Liu, W., Zhang, Y., Pan, Y., Wang, Z., Thomas, W. G., and Chen, Y. (2012) PAQR10 and PAQR11 mediate Ras signaling in the Golgi apparatus. *Cell Res* **22**, 661-676
43. Lorenzo, P. S., Kung, J. W., Bottorff, D. A., Garfield, S. H., Stone, J. C., and Blumberg, P. M. (2001) Phorbol esters modulate the Ras exchange factor RasGRP3. *Cancer Res* **61**, 943-949
44. Caloca, M. J., Zugaza, J. L., and Bustelo, X. R. (2003) Exchange factors of the RasGRP family mediate Ras activation in the Golgi. *J Biol Chem* **278**, 33465-33473
45. Bivona, T. G., Quatela, S. E., Bodemann, B. O., Ahearn, I. M., Soskis, M. J., Mor, A., Miura, J., Wiener, H. H., Wright, L., Saba, S. G., Yim, D., Fein, A., Perez de Castro, I., Li, C., Thompson, C. B., Cox, A. D., and Philips, M. R. (2006) PKC regulates a farnesyl-electrostatic switch on K-Ras that promotes its association with Bcl-XL on mitochondria and induces apoptosis. *Mol Cell* **21**, 481-493
46. Neel, N. F., Martin, T. D., Stratford, J. K., Zand, T. P., Reiner, D. J., and Der, C. J. (2011) The RalGEF-Ral Effector Signaling Network: The Road Less Traveled for Anti-Ras Drug Discovery. *Genes Cancer* **2**, 275-287
47. Varma, S., and Khandelwal, R. L. (2007) Effects of rapamycin on cell proliferation and phosphorylation of mTOR and p70(S6K) in HepG2 and HepG2 cells overexpressing constitutively active Akt/PKB. *Biochim Biophys Acta* **1770**, 71-78
48. Calimeri, T., and Ferreri, A. J. (2017) m-TOR inhibitors and their potential role in haematological malignancies. *Br J Haematol*
49. Claperon, A., and Therrien, M. (2007) KSR and CNK: two scaffolds regulating RAS-mediated RAF activation. *Oncogene* **26**, 3143-3158
50. Koveal, D., Schuh-Nuhfer, N., Ritt, D., Page, R., Morrison, D. K., and Peti, W. (2012) A CC-SAM, for coiled coil-sterile alpha motif, domain targets the scaffold KSR-1 to specific sites in the plasma membrane. *Sci Signal* **5**, ra94
51. Matallanas, D., Sanz-Moreno, V., Arozarena, I., Calvo, F., Agudo-Ibanez, L., Santos, E., Berciano, M. T., and Crespo, P. (2006) Distinct utilization of effectors and biological outcomes resulting from site-specific Ras activation: Ras functions in lipid rafts and Golgi complex are dispensable for proliferation and transformation. *Mol Cell Biol* **26**, 100-116
52. Gentry, L. R., Martin, T. D., Reiner, D. J., and Der, C. J. (2014) Ral small GTPase signaling and oncogenesis: More than just 15minutes of fame. *Biochim Biophys Acta* **1843**, 2976-2988
53. Falsetti, S. C., Wang, D. A., Peng, H., Carrico, D., Cox, A. D., Der, C. J., Hamilton, A. D., and Sebt, S. M. (2007) Geranylgeranyltransferase I inhibitors target RalB to inhibit anchorage-dependent growth and induce apoptosis and RalA to inhibit anchorage-independent growth. *Mol Cell Biol* **27**, 8003-8014
54. Gentry, L. R., Nishimura, A., Cox, A. D., Martin, T. D., Tsygankov, D., Nishida, M., Elston, T. C., and Der, C. J. (2015) Divergent roles of CAAX motif-signaled posttranslational modifications in the regulation and subcellular localization of Ral GTPases. *J Biol Chem* **290**, 22851-22861
55. Diaz-Rohrer, B. B., Levental, K. R., Simons, K., and Levental, I. (2014) Membrane raft association is a determinant of plasma membrane localization. *Proc Natl Acad Sci U S A* **111**, 8500-8505

56. Levental, I., and Veatch, S. L. (2016) The Continuing Mystery of Lipid Rafts. *J Mol Biol* **428**, 4749-4764
57. Carquin, M., D'Auria, L., Pollet, H., Bongarzone, E. R., and Tyteca, D. (2016) Recent progress on lipid lateral heterogeneity in plasma membranes: From rafts to submicrometric domains. *Prog Lipid Res* **62**, 1-24
58. Gao, X., Lowry, P. R., Zhou, X., Depry, C., Wei, Z., Wong, G. W., and Zhang, J. (2011) PI3K/Akt signaling requires spatial compartmentalization in plasma membrane microdomains. *Proc Natl Acad Sci U S A* **108**, 14509-14514
59. Pike, L. J., and Miller, J. M. (1998) Cholesterol depletion delocalizes phosphatidylinositol bisphosphate and inhibits hormone-stimulated phosphatidylinositol turnover. *J Biol Chem* **273**, 22298-22304
60. van Rheenen, J., Achame, E. M., Janssen, H., Calafat, J., and Jalink, K. (2005) PIP2 signaling in lipid domains: a critical re-evaluation. *EMBO J* **24**, 1664-1673
61. Ji, C., Zhang, Y., Xu, P., Xu, T., and Lou, X. (2015) Nanoscale Landscape of Phosphoinositides Revealed by Specific Pleckstrin Homology (PH) Domains Using Single-molecule Superresolution Imaging in the Plasma Membrane. *J Biol Chem* **290**, 26978-26993
62. Roy, S., Plowman, S., Rotblat, B., Prior, I. A., Muncke, C., Grainger, S., Parton, R. G., Henis, Y. I., Kloog, Y., and Hancock, J. F. (2005) Individual palmitoyl residues serve distinct roles in H-ras trafficking, microlocalization, and signaling. *Mol Cell Biol* **25**, 6722-6733
63. Prior, I. A., Muncke, C., Parton, R. G., and Hancock, J. F. (2003) Direct visualization of Ras proteins in spatially distinct cell surface microdomains. *J Cell Biol* **160**, 165-170
64. Abankwa, D., Gorge, A. A., Inder, K., and Hancock, J. F. (2010) Ras membrane orientation and nanodomain localization generate isoform diversity. *Proc Natl Acad Sci U S A* **107**, 1130-1135
65. Woo, J., and von Arnim, A. G. (2008) Mutational optimization of the coelenterazine-dependent luciferase from Renilla. *Plant Methods* **4**, 23
66. Szentpetery, Z., Varnai, P., and Balla, T. (2010) Acute manipulation of Golgi phosphoinositides to assess their importance in cellular trafficking and signaling. *Proc Natl Acad Sci U S A* **107**, 8225-8230
67. Varnai, P., Toth, B., Toth, D. J., Hunyady, L., and Balla, T. (2007) Visualization and manipulation of plasma membrane-endoplasmic reticulum contact sites indicates the presence of additional molecular components within the STIM1-Orai1 Complex. *J Biol Chem* **282**, 29678-29690
68. Balla, T., Bondeva, T., and Varnai, P. (2000) How accurately can we image inositol lipids in living cells? *Trends Pharmacol Sci* **21**, 238-241

Figure legends

Figure 1. *Constructs and molecular approach used in the study*

(A) N- or C-terminal target sequences of various proteins were used to generate PM localized Venus proteins. The panel on the top shows the targeted Venus proteins on a schematic drawing. The table demonstrates the sequences and the type of occurred lipid modifications of the applied targeting signals. The amino acids are highlighted in the sequences where the distinct modifications befall. Palmitoylation (blue) occurs on cysteine residues without a preference of placement, myristoylation (green) happens always on the N-terminal glycine residues after the first methionine, prenylation (brown) occurs on the C-terminal half of the proteins within the CAAX domain. Polybasic cluster regions are highlighted in red by the c-Src₁₋₁₅ and K-Ras-CAAX constructs. Confocal images reveal the intracellular localization of the PM targeted Venus proteins transiently expressed in HEK 293T cells.

(B) Schematic illustration of the proposed BRET measurements used to follow the intracellular trafficking of the PM bound Venus constructs after their release from the PM.

(C) Localization sequences or full length proteins were used to target the Luciferase enzyme to the cytoplasmic surface of various endomembrane (EM) compartment (Golgi: trans-Golgi compartment, mito: mitochondrion, ER: endoplasmic reticulum, EE: early endosome). In order to verify their proper endomembrane localization with confocal microscopy, HEK 293T cells were transiently transfected with constructs, in which luciferase was replaced by Cerulean.

Figure 2. *PM PPIs depletion achieved via rapamycin induced recruiting of the bifunctional PPIs phosphatase Pseudojanin (PJ) or by using the PI3K inhibitor wortmannin*

(A) Schematic representation of the PM PPIs depletion system. After rapamycin treatment, the cytoplasmic, FKBP-fused bifunctional phosphatase, PJ, binds to the PM anchored FRB. The recruitment of PJ is expected to cause a rapid degradation of the PM PPIs, resulting low levels of polyphosphorilated forms (PtdIns4P, PtdIns(4,5)P₂, PtdIns(3,4,5)P₃) and concomitant elevation of phosphatidyl inositol (PtdIns). Wortmannin (100 nM) inhibits PI3K activity, suitable to prevent the phosphorylation of PtdIns(4,5)P₂ to PtdIns(3,4,5)P₃.

(B) Monitoring of the PM PPIs levels using fluorescently tagged specific lipid binding domains, as lipid sensors. The confocal images were collected from transiently transfected HEK 293T cells expressing the proteins of the lipid depletion system (PM-FRB and mRFP-FKBP-PJ) and the specific lipid sensors: SidM-2xP4M tagged with Cerulean (left) and the PLCδ1-PH (middle) domain tagged with Venus are suitable to recognize PM PtdIns4P and PtdIns(4,5)P₂, respectively. After rapamycin (300 nM) treatment, the cytoplasmic bifunctional phosphatase, PJ, is recruited to the PM, whereas the lipid binding domains are released from the PM indicating the effective PM PPIs depletion. The images were collected before and after the addition of rapamycin (300 nM, 5 min). Note that the SidM-2xP4M domain recognize PtdIns4P pools throughout the cells, therefore it become mostly Golgi localized after depleting PM PtdIns4P pools. Cells are representatives of at least ten measurements carried out in three independent experiments.

(C) Monitoring of the PPIs levels using recently developed specific BRET-based biosensors capable to measure PM lipid levels (24). The measurements were carried out on transiently transfected HEK 293T cells expressing the proteins of the depletion system (PM-FRB and mRFP-FKBP-PJ) and the various biosensors: L10-Venus-T2A-Luc-SidM-2xP4 for PM PtdIns4P, L10-Venus-T2A-PLCδ1-PH-Luc for PM PtdIns(4,5)P₂ and L10-Venus-T2A-Btk-PH-Luc for PM PtdIns(3,4,5)P₃ measurements. Wortmannin (Wm) was applied in a concentration of 100 nM, in which it inhibits PI3 but no PI4 kinases. The lipid depletion system was activated by 300 nM rapamycin. BRET ratio values were normalized by considering the resting ratio as 100% and the complete lack of energy transfer as 0% (see details of the calculation in Materials and Methods). Data are means ± SEM of three independent experiments.

Figure 3. *Effect of PM PPIs depletion on the rearrangement of various PM-targeted Venus proteins*

(A) Monitoring of the translocation of various PM targeted Venus constructs in transiently transfected HEK 293T cells also expressing the proteins of the lipid depletion system (PM-FRB and mRFP-FKBP-PJ).

Confocal images were taken before and after the rapamycin treatment (300 nM 5 min). Cells are representatives of at least ten measurements carried out in three independent experiments.

(B-D) BRET measurements to examine the interaction between various PM targeted Venus proteins and endoplasmic reticulum targeted Luciferase construct (Luc-ER) (B), between K-Ras-CAAX tagged Venus and early endosome (Luc-EE), mitochondria (Mito-Luc) and trans-Golgi (Golgi-Luc) targeted Luciferase constructs (C) and between H-Ras-CAAX tagged Venus and trans-Golgi targeted Luciferase construct (Golgi-Luc) (D). The measurements were carried out on transiently transfected HEK 293T cells also expressing the proteins of the depletion system (PM-FRB-mRFP and mRFP-FKBP-PJ). The lipid depletion system was activated by 300 nM rapamycin. BRET ratio values are expressed as difference between rapamycin treated and vehicle (DMSO) treated cells. Data are means \pm SEM of three independent experiments. Statistical analysis were performed using t-test to compare the mean of the last three data points before and after the stimulation $*p < 0.05$, $***p < 0.001$; ns, non-significant.

Figure 4. Investigation of the travel route of the K-Ras-CAAX tagged Venus protein to the Golgi, and evaluation of the significance of the PtdIns4P content of this membrane in the translocation process

(A) Interaction between the Venus-K-Ras-CAAX and Golgi-Luc proteins by BRET was measured in HEK 293T cells also expressing the proteins of the depletion system (PM-FRB-mRFP and mRFP-FKBP-PJ). Lipid depletion was activated by 300 nM rapamycin. Deltarasin pretreatment (10 μ M, 10 min) was used to competitively inhibit the binding of the Venus-K-Ras-CAAX proteins to their solubilizing factor molecule PDE δ , which promotes their trafficking procedure. BRET ratio values are expressed as difference between rapamycin treated and vehicle (DMSO) treated cells in the case of both the untreated or deltarasin pretreated cells. Data are means \pm SEM of three independent experiments. Statistical analysis were performed using t-test ($*p < 0.05$, $**p < 0.01$).

(B) Intracellular distribution of Venus-K-Ras-CAAX was examined by confocal microscopy in COS-7 cells also expressing the proteins of the lipid depletion system (PM-FRB and mRFP-FKBP-PJ). The images were collected before and 5 min after the addition of 300 nM rapamycin. Cells are representatives of at least ten measurements carried out in three independent experiments.

(C) Intracellular distribution of Venus-K-Ras-CAAX was examined by confocal microscopy in COS-7 cells also expressing the proteins of the lipid depletion system (PM-FRB and mRFP-FKBP-PJ). Deltarasin treatment of the cells (10 μ M, 5 min) was followed by the activation of the lipid depletion system by adding rapamycin (300 nM, 5 min). Note the increased number of intracellular vesicles instead of the Golgi localization of Venus-K-Ras-CAAX. Cells are representatives of at least six measurements carried out in three independent experiments.

(D) The effect of PM permeabilization was examined in HeLa cells transiently expressing Venus-K-Ras-CAAX or Venus-H-Ras-CAAX. HeLa cells were kept in an intracellular solution during the measurement. Permeabilization was achieved by adding digitonin (25 μ g/ml, 5 min). Note the appearance of the fluorescent signal on the membrane of non-transfected cells in the case of Venus-K-Ras-CAAX, but not in Venus-H-Ras-CAAX. Cells are representatives of at least six measurements carried out in two independent experiments.

(E) The effect of the combined PM and Golgi PPIs depletion on the BRET signal was measured between the Venus-K-Ras-CAAX and Golgi-Luc proteins (upper graph). In addition to these proteins, HEK 293T cells also expressed the proteins of the PM lipid depletion (PM-FRB-mRFP and mRFP-FKBP-PJ). To achieve a combined depletion of PtdIns4P also in the Golgi compartment (PM + Golgi PPIs depletion), cells were also transfected with TGN38-FRB-mRFP as an additional anchor of PJ on the surface of Golgi (see inset). For control TGN38-mRFP was used instead of TGN38-FRB-mRFP. BRET ratio values are expressed as difference between rapamycin treated and vehicle (DMSO) treated cells. In parallel, on the same plate, PM PtdIns(4,5) P_2 levels was also measured. For this, cells expressed Venus and luciferase tagged PLC δ 1-PH instead of Venus-K-Ras-CAAX and Golgi-Luc proteins. BRET ratio values were normalized by considering the resting ratio as 100% and the complete lack of energy transfer as 0% (see details of the calculation in Materials and Methods). Data are means \pm SEM of three independent experiments. Statistical analysis were performed using t-test ($*p < 0.05$, $**p < 0.01$).

Figure 5. Effect of the isolated depletion of various types of PPIs on the K-Ras-CAAX translocation

(A) To examine the effect of PM PtdIns(3,4,5) P_3 on the K-Ras-CAAX translocation to the Golgi. BRET measurements were carried out on transiently transfected HEK 293T cells, expressing the required proteins (PM-FRB-mRFP and mRFP-FKBP-PJ) of the depletion system, and the Venus-K-Ras-CAAX and Golgi-Luc proteins. PM PPIs was evoked by adding rapamycin (300 nM) or/and the PI3K inhibitor wortmannin (100 nM). The difference of the BRET ratios was calculated between the stimulated and vehicle (DMSO) treated cells. Data are means \pm SEM of three independent experiments. Statistical analysis were performed using *t*-test in the case of the individual curves, and one way ANOVA was executed to examine the differences between the distinct treatments ($*p < 0.05$, $**p < 0.01$; ns, non-significant).

(B) Effect of the solely PM PtdIns4 P (green) or PtdIns(4,5) P_2 (red) depletion compared to the joint (blue) depletion on the Venus-K-Ras-CAAX translocation to the Golgi, achieved via recruiting distinct specificity phosphatases (FKBP-PJ for PtdIns4 P and PtdIns(4,5) P_2 ; FKBP-PJ-Sac1 for PtdIns4 P and FKBP-PJ-5ptase for PtdIns(4,5) P_2 depletion) to the PM anchored FRB protein (PM-FRB-mRFP) by 300 nM rapamycin treatment. The experiments were carried out on transiently transfected HEK 293T cells. PM PPIs levels were also monitored simultaneously with translocation experiments using the same specific BRET based biosensors which were presented on Fig. 2C. The lipid changes were only plotted in the case of FKBP-5ptase (red) or FKBP-4ptase (green). (The results of the joint depletion on the lipid pools were previously demonstrated also on the Fig. 2C.) The difference of the BRET ratios was calculated between rapamycin (300 nM) and vehicle (DMSO) treated cells. BRET ratio values were normalized by considering the resting ratio as 100% and the complete lack of energy transfer as 0% (see details of the calculation in Materials and Methods). Data are means \pm SEM of four independent experiments. Statistical analysis were performed using *t*-test in the case of the individual curves, and one way ANOVA was executed to examine the differences between the different conditions ($**p < 0.01$, $***p < 0.001$).

Figure 6. Investigation of the localization of the constitutively active full-length forms of fluorescently tagged K- and H-Ras constructs after PM PPIs depletion

(A) Schematic representation of the full-length K- and H-Ras-G12V constructs tagged with Venus fluorescent protein at the N-terminus. Confocal images show transiently transfected HEK 293T cells expressing the Venus tagged K- (left panel) or H-Ras-G12V (right panel) constructs and the proteins of the PPIs depletion system (PM-FRB and mRFP-FKBP-PJ, not visible). The images were collected before (left) and 5 min after the activation of the PM PPIs depletion system with 300 nM rapamycin. Cells are representatives of at least ten measurements carried out in three independent experiments.

(B-C) Effect of the PM PPIs depletion on the K-Ras G12V or H-Ras G12V interaction with the endoplasmic reticulum or Golgi membrane (ER). BRET was measured between Venus tagged full-length Ras constructs and the same ER or Golgi targeted Luciferase protein as by the measurement on the Fig. 3C (ER-Luc on Panel B, and Golgi-Luc on Panel C). The measurements were carried out on transiently transfected HEK 293T cells expressing the indicated constructs for the BRET measurements and the proteins of the depletion system (PM-FRB-mRFP and mRFP-FKBP-PJ). BRET ratios were calculated between rapamycin (300 nM) and vehicle (DMSO) treated cells. Data are means \pm SEM of three independent experiments. Statistical analysis were performed using *t*-test ($*p < 0.05$, ns, non-significant).

Figure 7. Localization of the Venus-K-Ras-CAAX and Venus-K-Ras G12V constructs after PM PPIs depletion achieved via Gq-coupled 7-TM receptor activation

(A) BRET measurements represent the interaction between the Venus-K-Ras-CAAX or Venus-K-Ras-G12V constructs and Golgi targeted Luciferase (Golgi-Luc) after treating the cells with carbachol (10 μ M) (blue plot). The specific inhibitor against PI4KA (responsible for PM PtdIns4 P resynthesis) were also applied (A1 compound, in 10 nM concentration, 10 min pretreatment, red plot) in these experiments. The experiments were carried out on transiently transfected HEK 293T cells, which were expressing the wild type muscarinic M3 receptor to achieve sufficient PM PPIs depletion after carbachol treatment. The difference of the BRET ratios was calculated between carbachol (10 μ M) treated and untreated cells. The

data are means \pm SEM of three independent experiments. Statistical analysis were performed using *t*-test. Because of the different kinetic changes of the measurements without any pretreatment, *t*-test was also executed on the mean values of the three data points at the peak change (\sim 1 min after stimulation) ($*p < 0.05$, $**p < 0.01$, ns, non-significant).

(B) Parallel confocal images from cells expressing the Venus-K-Ras-CAAX construct show the same experiments which were presented on the panel A on the top. To evaluate the changes on the Golgi, transiently transfected COS-7 cells were applied aiming better insight to this region of the cells. Left pictures show the control period, middle images were collected 1 min after carbachol (10 μ M) treatment, and the right pictures represents the cells after 5 min of muscarinic receptor activation. Arrows indicate the position of the Golgi. The cells were expressing the wild type muscarinic M3 receptor, to achieve sufficient PM PPIs depletion after carbachol treatment (not visible). Cells are representatives of at least ten measurements carried out in three independent experiments.

(C) BRET measurements represent the interaction between the Venus-K-Ras-CAAX construct and Golgi targeted Luciferase (Golgi-Luc) after treating the cells with EGF (100 ng/ml) (blue plot). Specific inhibitors against PI4KA (A1 compound, in 10 nM concentration, 10 min pretreatment, red plot) and against the PI3K (wortmannin -indicated as Wm- in 100 nM concentration, 10 min pretreatment, green plot) were also applied in these experiments. The experiments were carried out on transiently transfected HEK 293T cells, which were expressing the human EGF receptor to achieve sufficient PM PPIs depletion after EGF treatment. The difference of the BRET ratios was calculated between EGF (100 ng/ml) treated and untreated cells. The data are means \pm SEM of four independent experiments. Statistical analysis were performed using *t*-test ($**p < 0.01$).

Figure 8. Measurement of the radiolabeled [3 H]-Leucine incorporation in distinct Ras mutants expressing cells with or without concomitant PM PPIs depletion

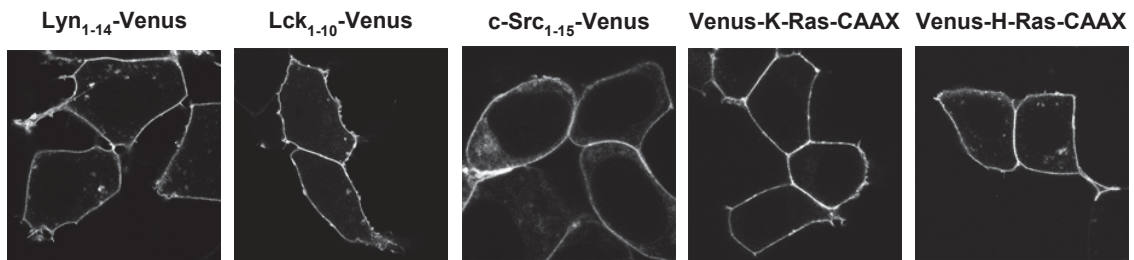
(A) Evaluation of the normalized 24 hour [3 H]-Leucine incorporation in transiently transfected COS-7 cells expressing the mRFP-tagged versions of the dominant negative S17N or constitutively active G12V forms of both K- and H-Ras proteins. Values were normalized to K-Ras S17N. Data are means \pm SEM of three independent experiments. Statistical analysis was carried out using two-way ANOVA followed by Holm-Sidak all pairwise multiple comparison method on the data of the four groups ($***p < 0.001$).

(B) Comparison of the normalized [3 H]-Leucine incorporation in distinct Ras isoforms expressing cells with or without concomitant PM PPIs. The measurements were carried out on transiently transfected COS-7 cells expressing the mRFP tagged versions of the indicated Ras isoforms and the required proteins of our PM PPIs depletion system (PM-FRB-mRFP and mRFP-FKBP-PJ). PM PPIs depletion was evoked by long term rapamycin treatment (100 nM, 24 hours, repeated in every 8 hours). For the control measurements, an enzymatically inactive form of the phosphatase was used (PJ-dead). Values were normalized to K-Ras S17N with PJ-dead recruitment. Data are means \pm SEM of four independent experiments. Statistical analysis was carried out using two-way ANOVA followed by Holm-Sidak all pairwise multiple comparison method on the data of the four groups ($**p < 0.01$, $***p < 0.001$, ns, non-significant).

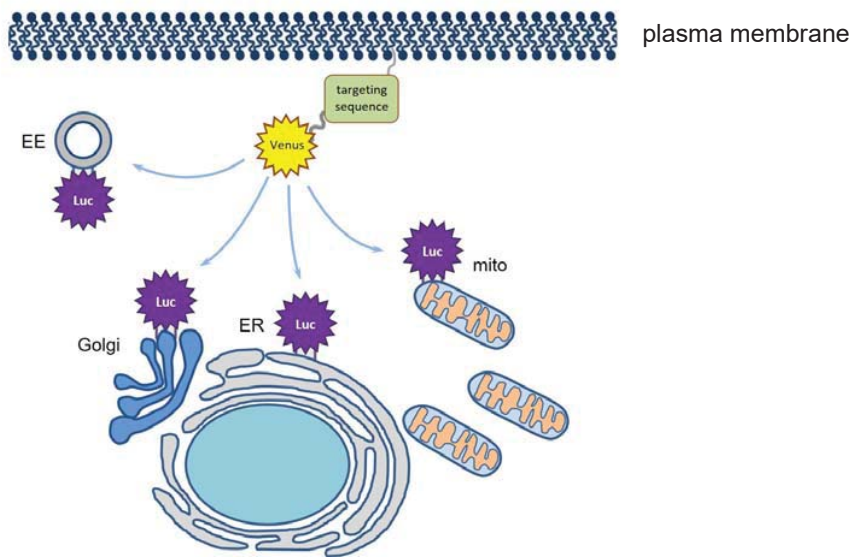
A



Targeting sequence	Type of modifications			
	Palmitoylation	Myristoylation	Prenylation	Polybasic cluster
Lyn ₁₋₁₄ : MGCIKSKGKDSAGA	*	*		
Lck ₁₋₁₀ : MGCVCSSNPE	**	*		
c-Src ₁₋₁₅ : MGSSKSKPKDPSQRR		*		*
K-Ras-CAAX : KEKMSKDGKKKKKSKTK-CVIM			*	*
H-Ras-CAAX : LRKLNPPDESGPGCMSCK-CVLS	**		*	



B



C

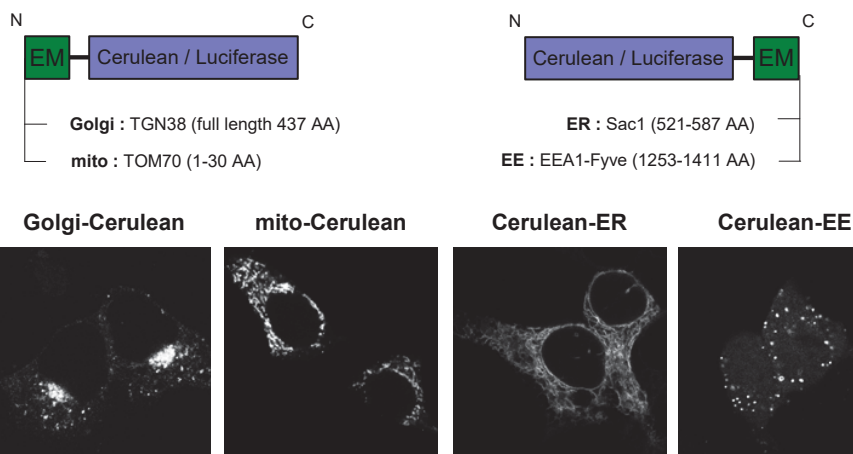


Figure 1

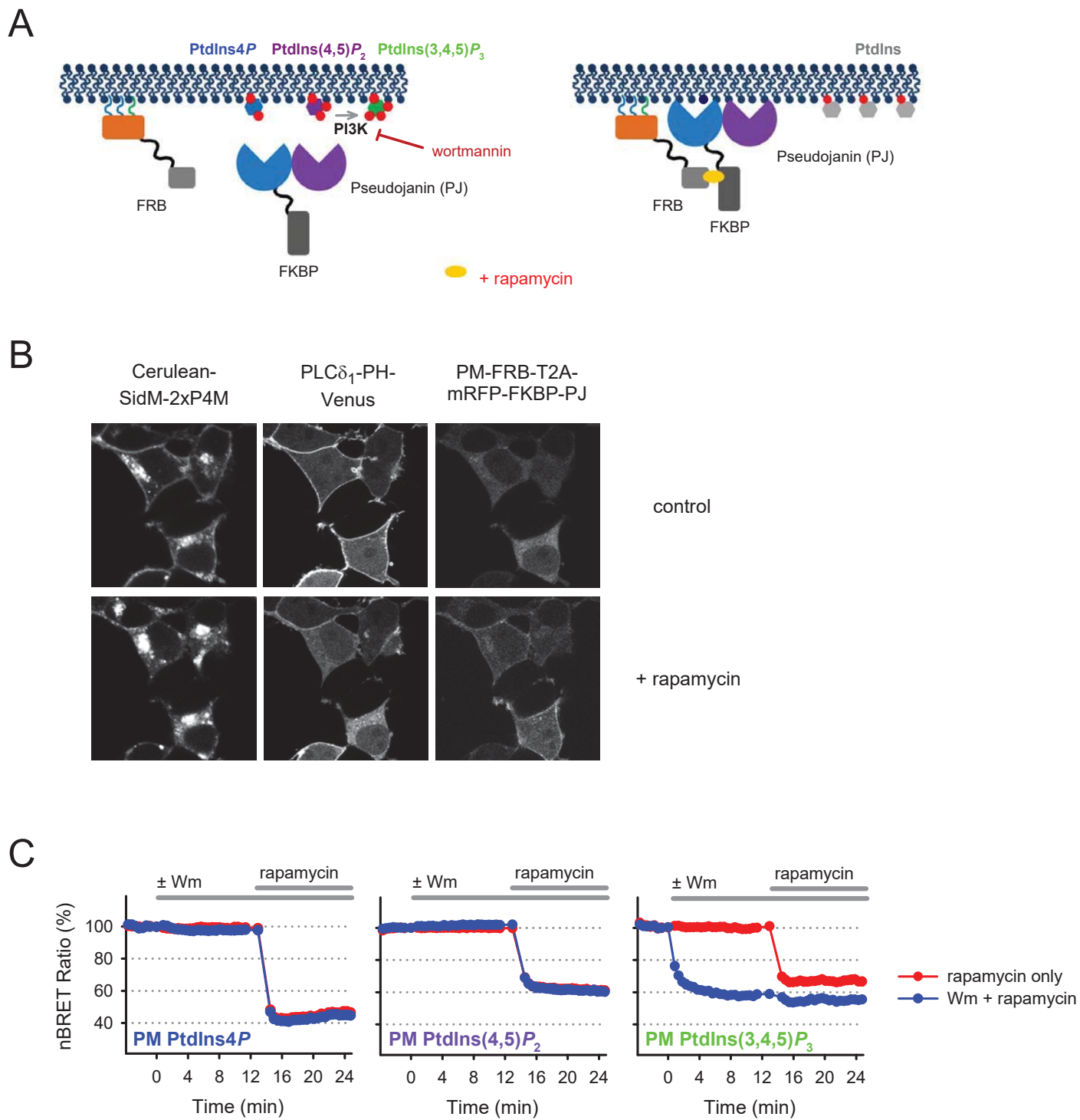
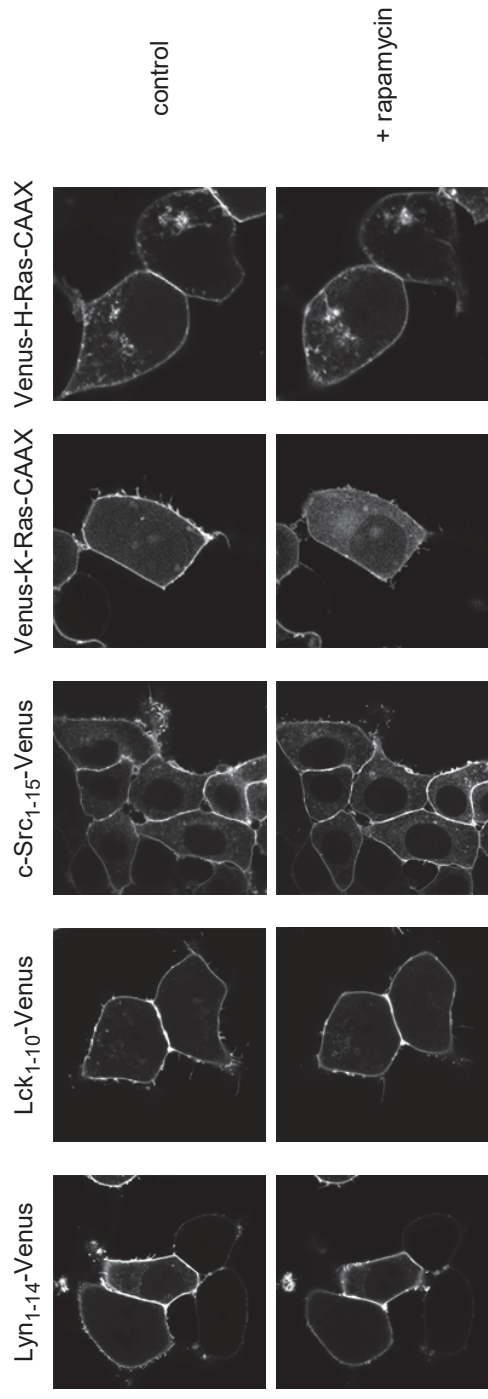
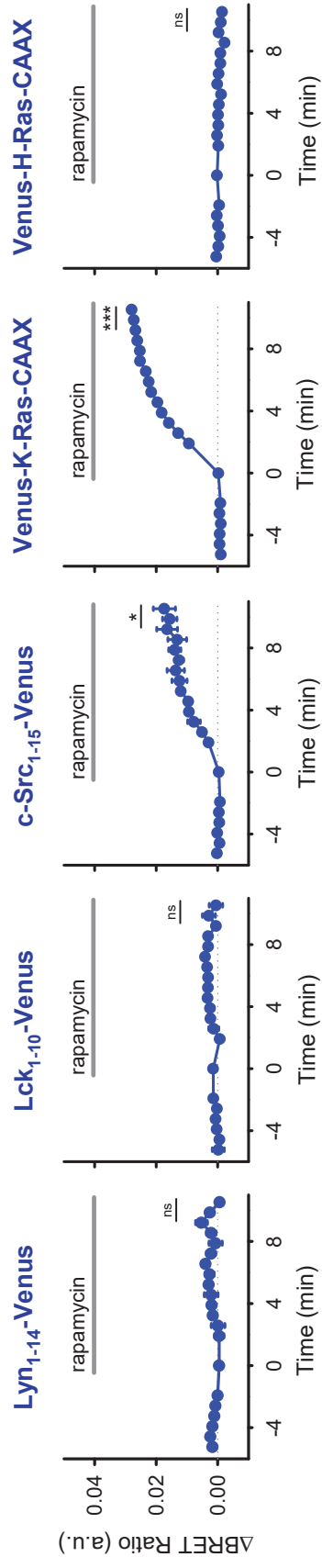
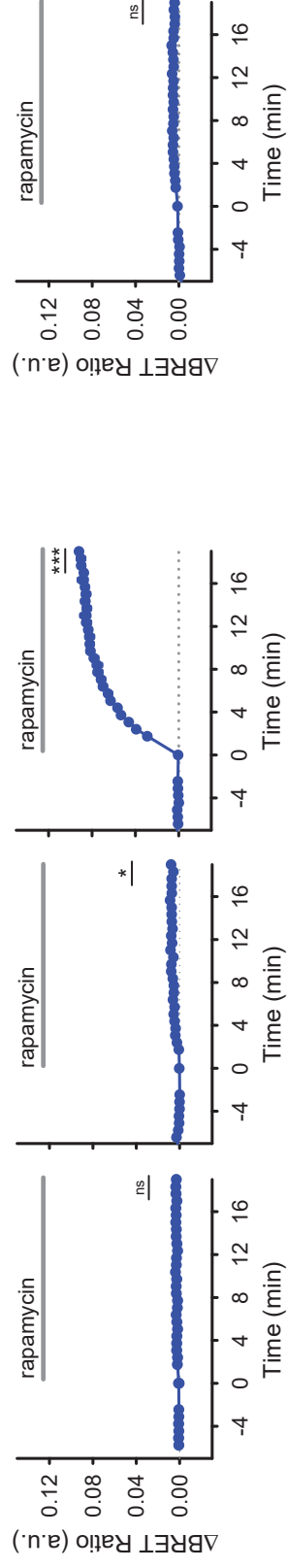
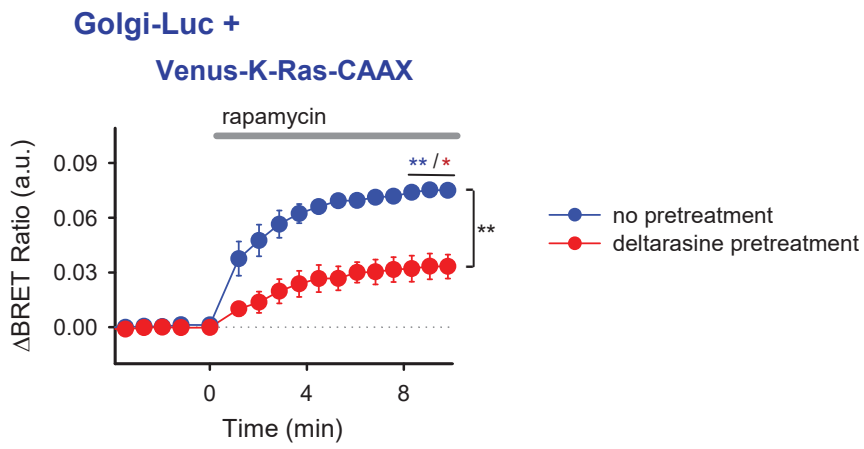
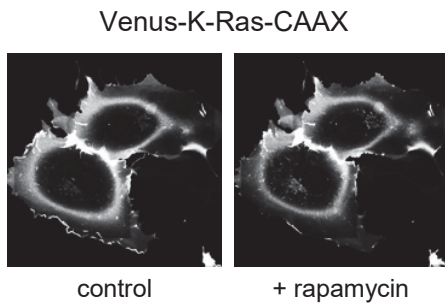
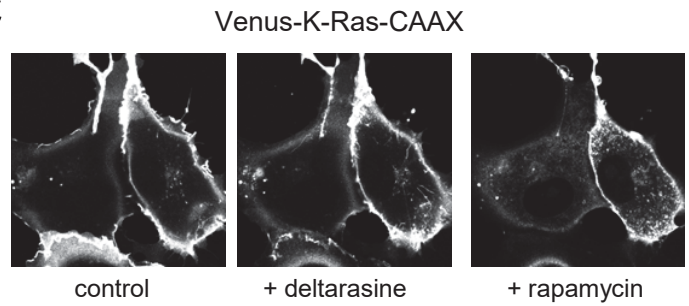
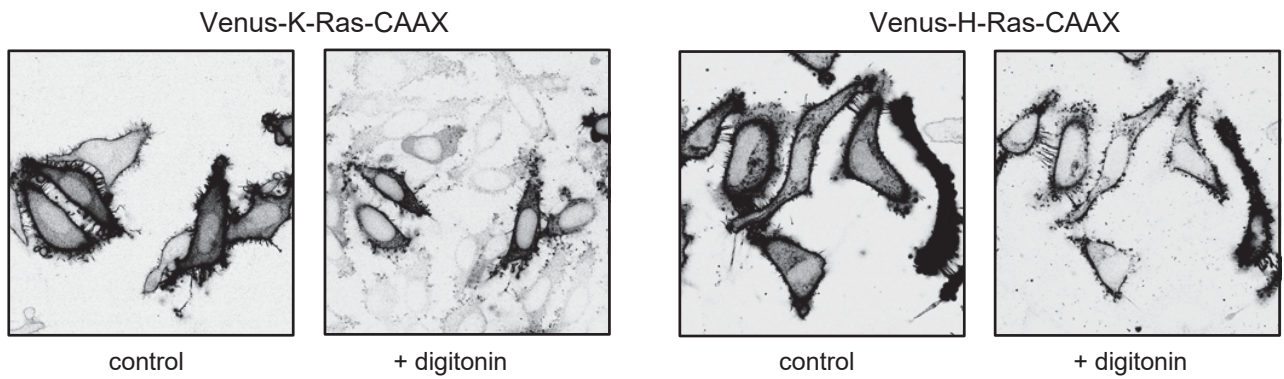
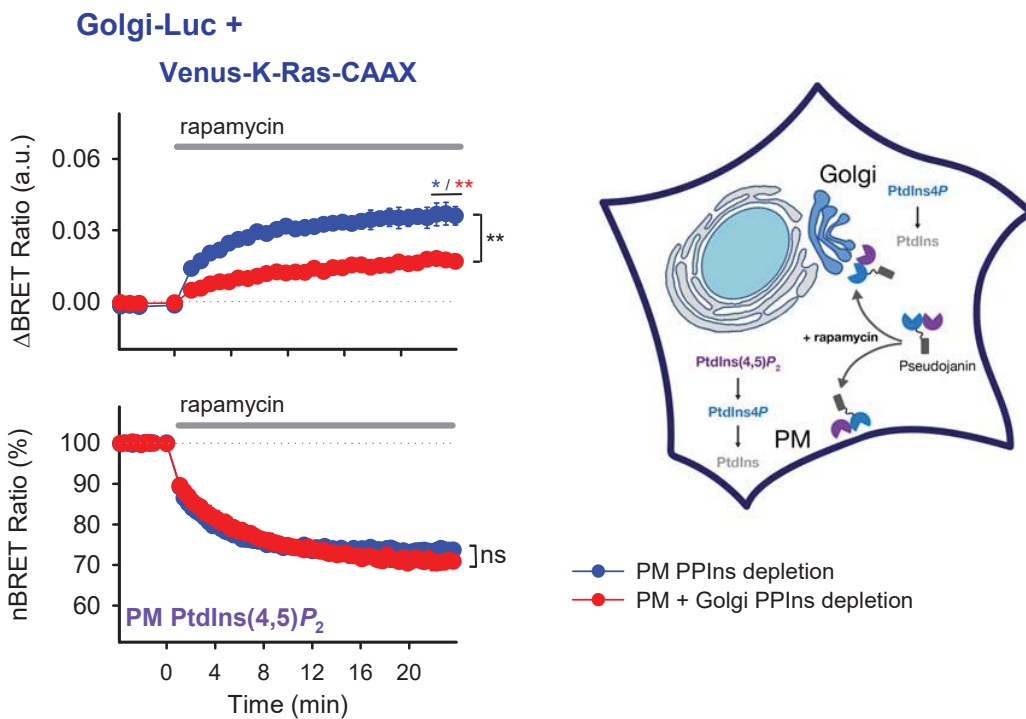


Figure 2

A**B****Luc-ER +****C****Luc-EE +****mito-Luc +****Golgi-Luc +****Venus-K-Ras-CAAX****Venus-K-Ras-CAAX****Venus-H-Ras-CAAX**

A**B****C****D****E****Figure 4**

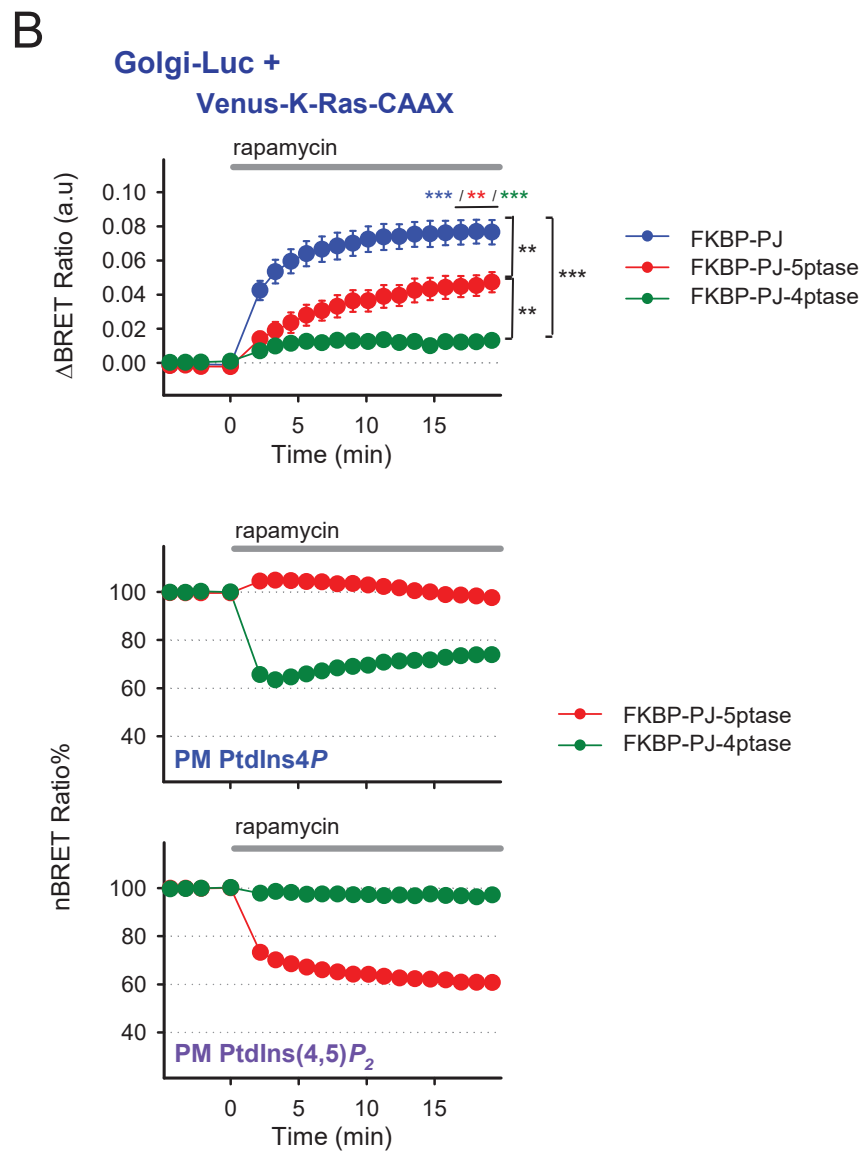
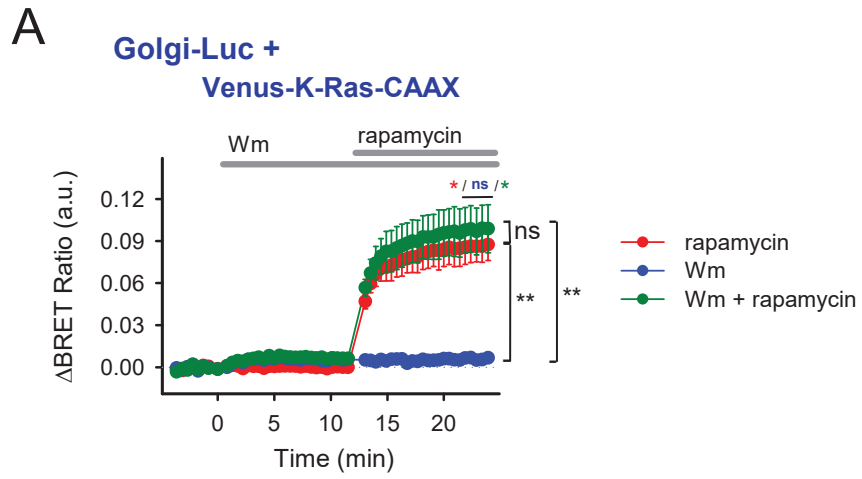


Figure 5

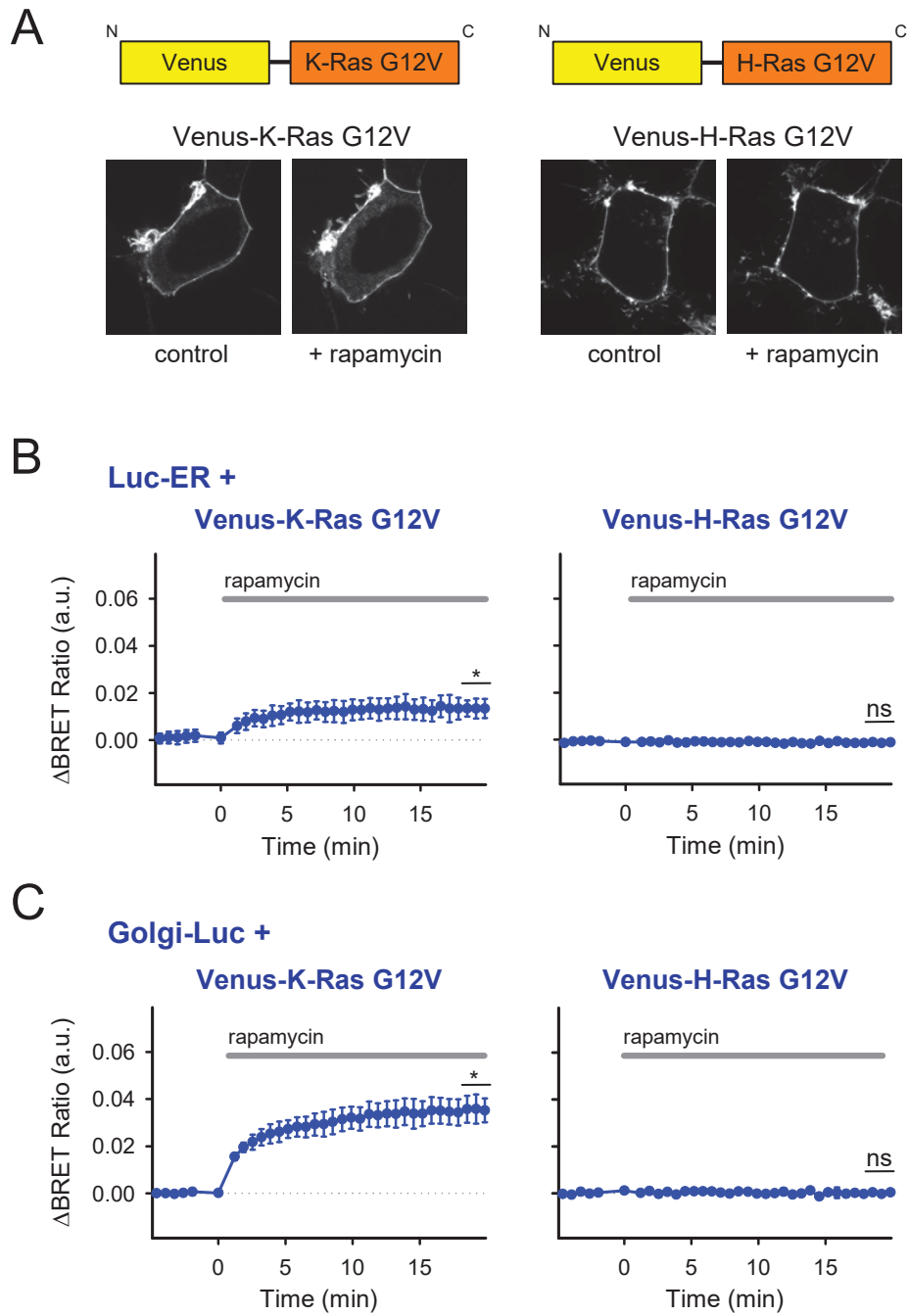


Figure 6

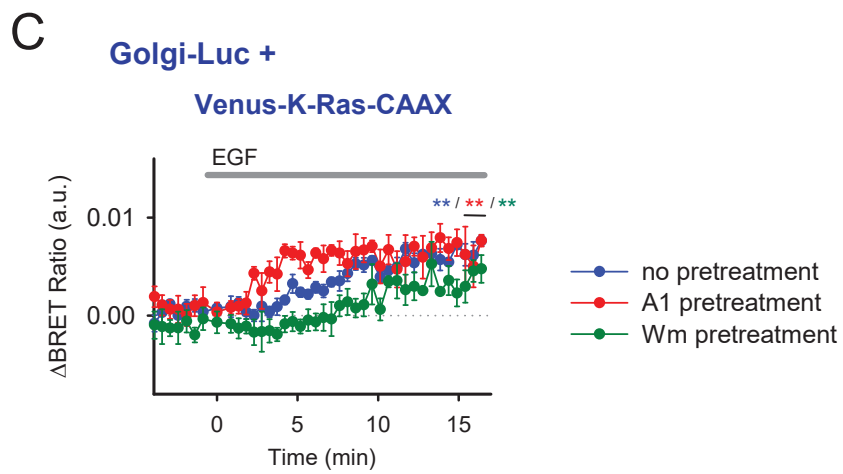
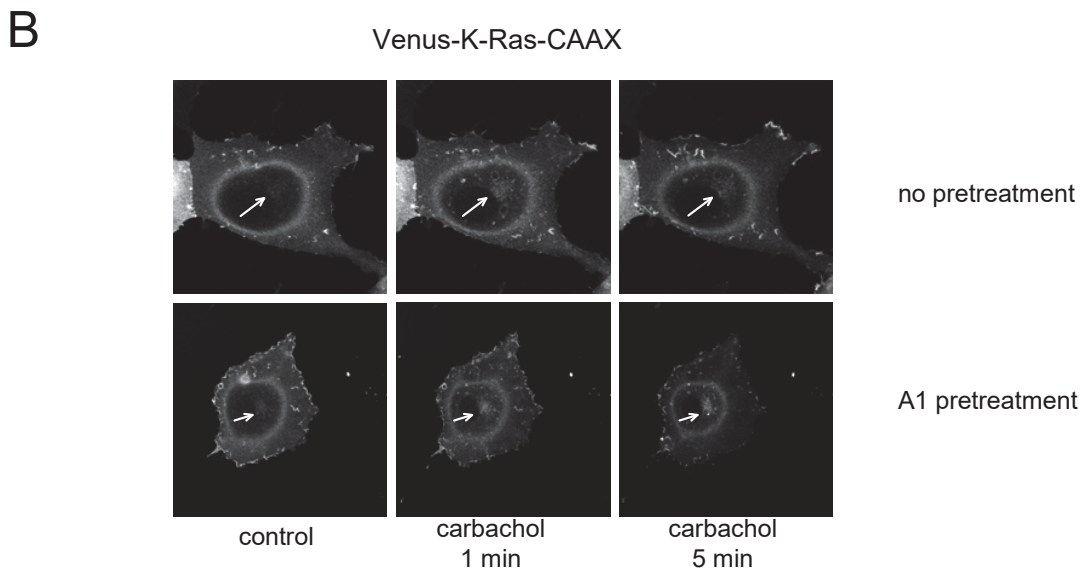
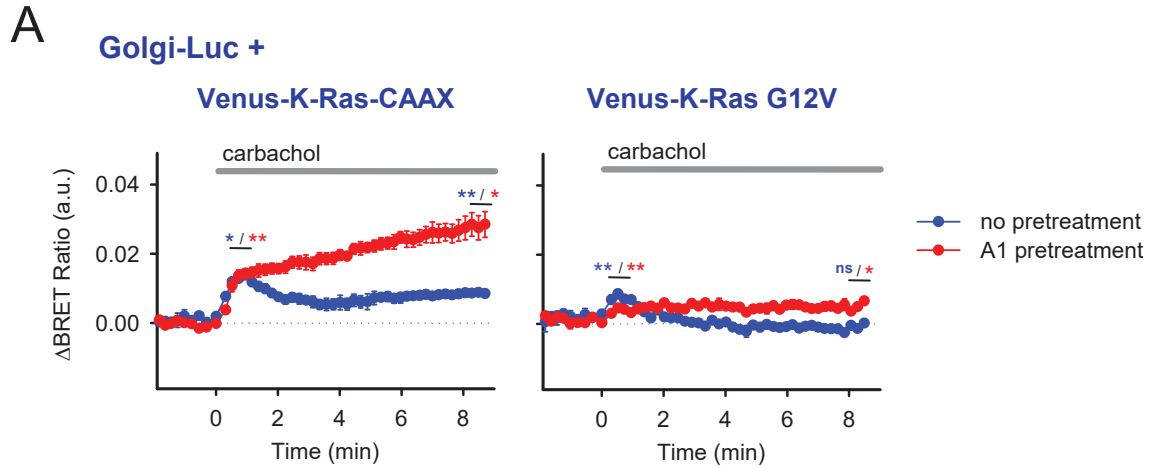


Figure 7

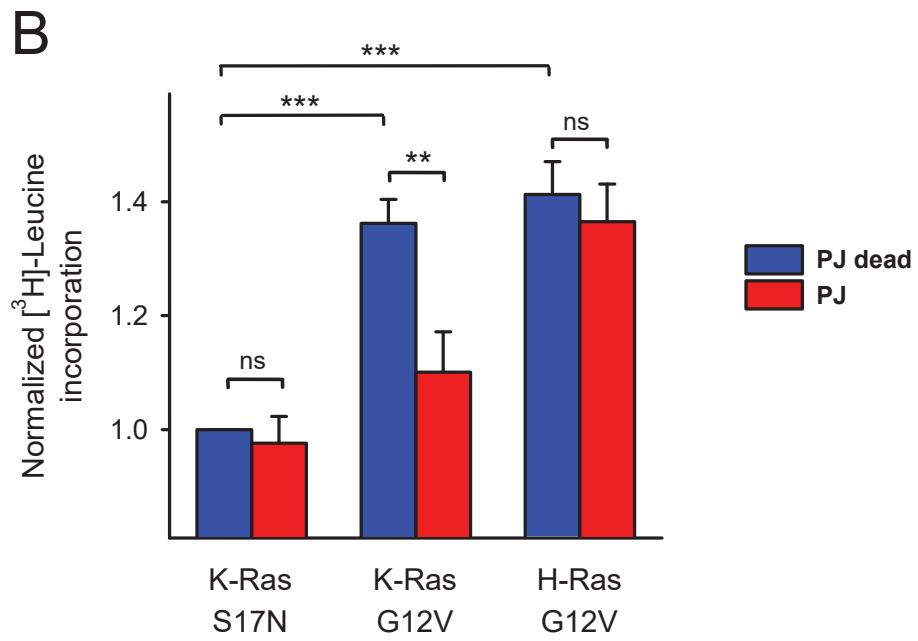
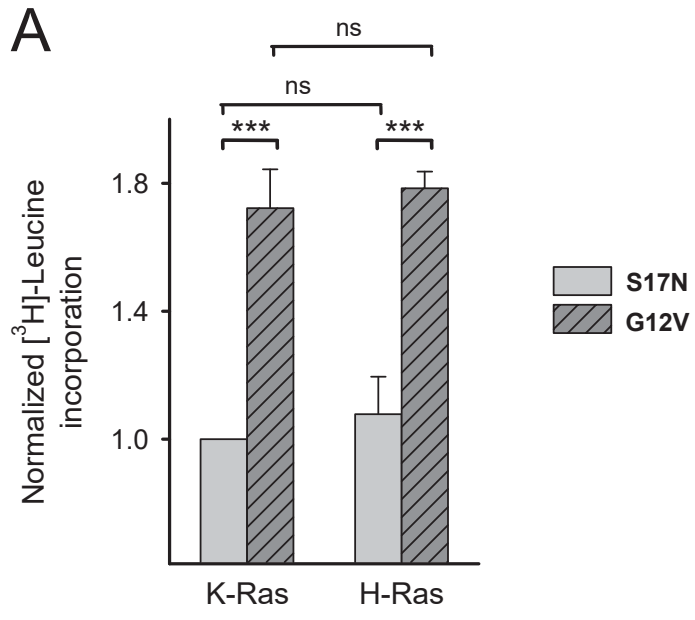


Figure 8